

This is a repository copy of *Leishmania genome dynamics during environmental adaptation reveals strain-specific differences in gene copy number variation, karyotype instability, and telomeric amplification*.

White Rose Research Online URL for this paper:

<https://eprints.whiterose.ac.uk/135934/>

Version: Accepted Version

Article:

Bussotti, Giovanni, Gouzelou, Evi, Cortes Boite, Mariana et al. (27 more authors) (2018) *Leishmania genome dynamics during environmental adaptation reveals strain-specific differences in gene copy number variation, karyotype instability, and telomeric amplification*. MBio. e01399-18. ISSN 2150-7511

<https://doi.org/10.1128/mBio.01399-18>

Reuse

This article is distributed under the terms of the Creative Commons Attribution (CC BY) licence. This licence allows you to distribute, remix, tweak, and build upon the work, even commercially, as long as you credit the authors for the original work. More information and the full terms of the licence here:

<https://creativecommons.org/licenses/>

Takedown

If you consider content in White Rose Research Online to be in breach of UK law, please notify us by emailing eprints@whiterose.ac.uk including the URL of the record and the reason for the withdrawal request.

1 ***Leishmania* genome dynamics during environmental adaptation reveals**
2 **strain-specific differences in gene copy number variation, karyotype**
3 **instability, and telomeric amplification**

4
5 Giovanni Bussotti^{1,2}, Evi Gouzelou², Mariana Côrtes Boité³, Ihsen Kherachi⁴, Zoubir Harrat⁴,
6 Naouel Eddaikra⁴, Jeremy C. Mottram⁵, Maria Antoniou⁶, Vasiliki Christodoulou⁶, Aymen
7 Bali^{7,8}, Fatma Z Guerfali^{7,8}, Dhafer Laouini^{7,8}, Maowia Mukhtar⁹, Franck Dumetz¹⁰, Jean-
8 Claude Dujardin^{10,11}, Despina Smirlis¹², Pierre Lechat¹, Pascale Pescher², Adil El Hamouchi¹³,
9 Meryem Lemrani¹³, Carmen Chicharro¹⁴, Ivonne Pamela Llanes-Acevedo¹⁴, Laura Botana¹⁴,
10 Israel Cruz¹⁴, Javier Moreno¹⁴, Fakhri Jeddi^{8,15}, Karim Aoun^{8,15}, Aïda Bouratbine^{8,15}, Elisa
11 Cupolillo³ and Gerald F. Späth^{2,*}

12 ¹Institut Pasteur – Bioinformatics and Biostatistics Hub – C3BI, USR 3756 IP CNRS – Paris,
13 France; ²Unité de Parasitologie moléculaire et Signalisation, Institut Pasteur, Paris, France;
14 ³Laboratory on Leishmaniasis Research, Oswaldo Cruz Institute-Fiocruz, Rio de Janeiro,
15 Brazil; ⁴Laboratoire d'Eco-épidémiologie parasitaire et Génétique des populations, Institut
16 Pasteur d'Alger, Alger, Algérie; ⁵Centre for Immunology and Infection, Department of
17 Biology, University of York, United Kingdom; ⁶Laboratory of Clinical Bacteriology,
18 Parasitology, Zoonoses and Geographical Medicine, School of Medicine, University of Crete,
19 Vassilika Vouton, Heraklion, Greece; ⁷Institut Pasteur de Tunis, LR11IPT02, Laboratory of
20 Transmission, Control and Immunobiology of Infections (LTCII), Tunis-Belvédère, Tunisia;
21 ⁸Université Tunis El Manar, Tunis, Tunisia; ⁹The Institute of Endemic Diseases, University of
22 Khartoum, Sudan; ¹⁰Molecular Parasitology Unit, Institute of Tropical Medicine, Antwerp,
23 Belgium; ¹¹Department of Biomedical Sciences, University of Antwerp, Belgium; ¹²Molecular
24 Parasitology Laboratory, Microbiology Department, Hellenic Pasteur Institute, Athens,

25 Greece; ¹³Laboratory of Parasitology and Vector-Borne-Diseases, Institut Pasteur du Maroc,
26 Casablanca, Morocco; ¹⁴WHO Collaborating Centre for Leishmaniasis, Instituto de Salud
27 Carlos III, Madrid, Spain; ¹⁵Institut Pasteur de Tunis, LR11IPT06, Research Laboratory
28 "Medical Parasitology, Biotechnology and Biomolecules", Tunis-Belvédère, Tunisia

29

30 * To whom correspondence should be addressed. Tel: +33.1.40.61.38.58; Fax:
31 +33.1.45.68.83.32; Email: gerald.spaeth@pasteur.fr

32

33 **Abstract**

34 Protozoan parasites of the genus *Leishmania* adapt to environmental change through chromosome
35 and gene copy number variations. Only little is known on external or intrinsic factors that
36 govern *Leishmania* genomic adaptation. Here, by conducting longitudinal genome analyses of ten
37 new *Leishmania* clinical isolates, we uncovered important differences in gene copy number among
38 genetically highly related strains and revealed gain and loss of gene copies as potential drivers of
39 long-term environmental adaptation in the field. In contrast, chromosome rather than gene
40 amplification was associated with short-term environmental adaptation to *in vitro* culture. Karyotypic
41 solutions were highly reproducible but unique for a given strain, suggesting that chromosome
42 amplification is under positive selection and dependent on species- and strain-specific, intrinsic
43 factors. We revealed a progressive increase in read depth towards the chromosome ends for various
44 *Leishmania* isolates, which may represent a non-classical mechanism of telomere maintenance that
45 can preserve integrity of chromosome ends during selection for fast *in vitro* growth. Together our
46 data draw a complex picture of *Leishmania* genomic adaptation in the field and in culture, which is
47 driven by a combination of intrinsic genetic factors that generate strain-specific, phenotypic
48 variations, which are under environmental selection and allow for fitness gain.

49

50 **Importance**

51 Protozoan parasites of the genus *Leishmania* cause severe human and veterinary diseases
52 world-wide, termed leishmaniasis. A hallmark of *Leishmania* biology is its capacity to adapt
53 to a variety of unpredictable fluctuations inside its human host, notably pharmacological
54 interventions thus causing drug resistance. Here we investigated mechanisms of
55 environmental adaptation using a comparative genomics approach by sequencing ten new
56 clinical isolates of the *L. donovani*, *L. major*, and *L. tropica* complexes that were sampled
57 across eight distinct geographical regions. Our data provide new evidence that parasites

58 adapt to environmental change in the field and in culture through a combination of
59 chromosome and gene amplification that likely causes phenotypic variation and drives
60 parasite fitness gains in response to environmental constraints. This novel form of gene
61 expression regulation through genomic change compensates for the absence of classical
62 transcriptional control in these early-branching eukaryotes and opens new venues for
63 biomarker discovery.

64

65 **Introduction**

66 Protozoan parasites of the genus *Leishmania* are transmitted by female blood-feeding sand
67 flies and can cause severe diseases in infected humans and animals. The success of this
68 pathogen relies on its capacity to sense changes in various host environments that trigger
69 various developmental transitions (1). Inside phlebotomine insect vectors, non-infectious
70 procyclic promastigote parasites differentiate into highly infectious metacyclic
71 promastigotes, which are transmitted to vertebrate hosts during a blood meal, where they
72 develop into the disease-causing amastigote form inside host macrophages (2, 3). Aside
73 from stage differentiation, *Leishmania* seem to adapt to a variety of environmental
74 fluctuations encountered in their hosts with important consequences for infection outcome,
75 such as drug treatment. Phenotypic shifts in *Leishmania* have been linked to genome
76 plasticity, with frequent copy number variations (CNVs) of individual genes or chromosomes
77 linked to drug resistance (4-9) or tissue tropism (10, 11). A better insight into molecular and
78 genetic mechanisms underlying *Leishmania* genetic diversity and evolution of new
79 phenotypes is therefore essential to understand parasite pathogenicity and hence the
80 epidemiology of *Leishmania* infection.

81 Combining DNaseq and RNAseq analyses of karyotypically distinct *L. donovani* field

82 isolates and experimental clones, we recently established a direct correlation between
83 transcript abundance and chromosome amplification (12, 13) - a form of genomic regulation
84 of gene expression levels that compensates for the absence of classical transcriptional
85 control in these early-branching eukaryotes (10, 14, 15). Using the *L. donovani* LD1S
86 experimental strain and conducting *in vitro* evolutionary experiments, we demonstrated the
87 highly dynamic, reversible and reproducible nature of parasite karyotypic changes, and
88 correlated chromosome amplification to fitness gains in culture (13). Using recent clinical
89 isolates of *L. donovani*, we demonstrated that such karyotypic changes were strain-specific
90 (12), suggesting a potential link between the genetic background of the parasite and its
91 karyotype plasticity (12, 16). Despite the potential relevance of genomic adaptation in
92 shaping the parasite pathogenic potential, only little is known about the dynamics of gene
93 and chromosome CNVs in *Leishmania* field isolates while they evolve to adapt to new
94 environments. Here we address this important open question by comparing the genomes of
95 ten clinical isolates belonging to three different *Leishmania* complexes (*L. donovani*, *L.*
96 *major*, *L. tropica*) from eight geographical regions. Read depth analysis revealed gene and
97 chromosome CNV as potential drivers of long-term and short-term adaptation, respectively.
98 Isolates during early and later stages of culture adaptation showed reproducible karyotypic
99 changes for a given strain, providing strong evidence that chromosomal amplification is
100 under positive selection. Significantly, these changes occurred in an individualized manner in
101 even highly related strains, thus implicating for the first time environment-independent
102 intrinsic genetic factors affecting *Leishmania* karyotypic adaptation.

103

104 **Material and Methods**

105 ***Leishmania* parasite isolation and culture.** Ten *Leishmania* strains belonging to the *L.*
106 *tropica*, *L. major* and *L. donovani* complexes of eight different geographical areas were
107 isolated from infected patients, dogs or hamster (**Table S1**). Some strains were
108 cryopreserved in liquid nitrogen prior to culture adaptation until used for this study (**Table**
109 **S1**). *Leishmania* isolates were first stabilized *in vitro* in media that were optimized in the
110 various LeiSHield partner laboratories ('Stabilization medium', **Table S2**), prior to expansion
111 in classical RPMI culture medium for a defined number of passages ('Expansion medium').
112 Seven strains belonging to the *L. donovani* complex were selected for the comparison of
113 intra-species evolvability in culture. These include the four *L. infantum* strains Linf_ZK27
114 from Tunisia, Linf_LLM56 and Linf_LLM45 from Spain, and Lin_02A from Brazil (voucher to
115 assess this sample at Coleção de Leishmania do Instituto Oswaldo Cruz (CLIOC): IOCL3598),
116 and the three *L. donovani* strains Ldo_BPK26 from India, Ldo_LTB from Sudan, and
117 Ldo_CH33 from Cyprus. The latter strain belongs to the *L. donovani* MON-37 zymodeme (17-
118 19) and multilocus microsatellite typing (MLMT) analysis has positioned it in a novel *L.*
119 *donovani sensulato* (s.l.) group (20). Our analysis further included two *L. major* strains
120 (Lmj_1948 from Tunisia, Lmj_A445 from Algeria) and one *L. tropica* strain (Ltr_16 from
121 Morocco) (**Table S1**). Genotyping methodologies were applied to confirm species identity of
122 the strains used in this work (**Table S1**). Standardized procedures for DNA sample
123 preparation and cell (sub)-culturing were used in all partner laboratories (**Table S2**).
124 Promastigotes from early cell culture (passage 2 of growth in Expansion medium, referred to
125 as early passage samples, EP) and derived parasites maintained in culture for three more *in*
126 *vitro* passages (EP+3) were processed for whole-genome sequencing (WGS) using parasites
127 from late logarithmic growth phase. While different *Leishmania* strains can show differences
128 in terms of generation time and can reach different population densities, we previously

129 estimated that a single passage in culture corresponds to ca. 10 generations (13). To
130 determine reproducibility of *in vitro* genome evolution, duplicate EP+3 samples (EP+3.1 and
131 EP+3.2) were generated for the Linf_ZK27, Lmj_1948, Lmj_A445, Ldo_BPK26 and Ltr_16
132 strains (**Figure S1**). Culture conditions and time in culture for the 25 samples are detailed in
133 **Table S2**.

134
135 **Nucleic acid extraction, sample preparation and sequencing analysis.** Procedures for DNA
136 sample preparation and quality control were standardized using common protocols. Briefly,
137 DNA extraction was performed using DNeasy blood and tissue kits from Qiagen according to
138 manufacturer instructions. Nucleic acid concentrations were measured with Qubit and the
139 DNA quality was evaluated on agarose gel. Between 2 to 5µg of DNA were used for
140 sequencing. The following samples showed low DNA amounts and were thus PCR amplified
141 before sequencing: Ldo_LTB_EP (five cycles), Ldo_LTB_EP+3 (five cycles), Linf_02A_EP (ten
142 cycles), Linf_02A_EP+3 (five cycles). No PCR amplification was performed for the other
143 samples.

144
145 Whole genome, short-insert, paired-end libraries were prepared for each sample.
146 Samples Ltr_16_EP, Ltr_16_EP+3.1, Ltr_16_EP+3.2, Ldo_BPK26_EP, Ldo_BPK26_EP+3.1,
147 Ldo_BPK26_EP+3.2, Lmj_A445_EP, Lmj_A445_EP+3.1, Lmj_A445_EP+3.2 were sequenced by
148 the Biomics sequencing platform (<https://research.pasteur.fr/en/team/biomics/>) with Hiseq
149 2500 rapid runs, resulting in 2×108bp reads using the NEXTflex PCR-Free kit. All other
150 samples were sequenced with the KAPA Hyper Prep Kit (Kapa Biosystems) at Centro
151 Nacional de Análisis Genómico (CNAG, <http://www.cnag.crg.eu/>) using the TruSeq SBS Kit
152 v3-HS (Illumina Inc.). Multiplex sequencing was performed according to standard Illumina

153 procedures, using a HiSeq2000 flowcell v3 generating 2×101bp paired-end reads. Reads
154 were deposited in the Sequence Read Archive database (SRA) database (21) and are publicly
155 available under the accession number SRP126578.

156

157 **Read alignment.** Gene annotations and reference genomes of *L.major* Friedlin and *L.*
158 *infantum* JPCM5 were downloaded from the Sanger FTP server (22) (URL
159 <ftp://ftp.sanger.ac.uk/pub/project/pathogens/gff3/CURRENT/>) on 09/05/2017, whereas
160 PacBio *L. donovani* LDBPK assembly and annotations were downloaded on 02/05/2017 (URL
161 <ftp://ftp.sanger.ac.uk/pub/project/pathogens/Leishmania/donovani/LdBPKPAC2016beta>).

162 The reads were aligned to the reference genomes with *BWA mem* (version 0.7.12) (23, 24)
163 with the flag -M to mark shorter split hits as secondary. *Samtools fixmate*, *sort*, and *index*
164 (25) (version 1.3) were used to process the alignment files and turn them into bam format.
165 *RealignerTargetCreator* and *IndelRealigner* from the *GATK* suite (26-28) were run to
166 homogenize indels. Eventually, PCR and optical duplicates were labeled with *Picard*
167 *MarkDuplicates* (<https://broadinstitute.github.io/picard/>, version 1.94 (1484)) using the
168 option 'VALIDATION_STRINGENCY=LENIENT'. While the reads were aligned against full
169 assemblies, including unsorted contigs, just the canonical 36 chromosomes were considered
170 for downstream analyses of ploidy estimation and copy number alterations. This filter was
171 necessary because of the high content of repetitive elements and the absence of
172 comparable and high quality annotations in the contigs. Given that the *L. tropica* reference
173 genome is still unfinished, the sample Ltr_16 was aligned against the *L. major* Friedlin
174 genome. Overall, starting from a total of 1,011,803,806 short reads, 952,093,114 were
175 successfully aligned to the respective reference genomes (**Table S3**). *Picard*
176 *CollectAlignmentSummaryMetrics* was used to estimate sequencing and mapping statistics.

177

178 **Comparative genome analysis.** Whole genome sequencing data from the EP *Leishmania*
179 isolates were processed with *Trimmomatic* (29) (version 0.35) to remove low quality bases
180 (options LEADING:3 TRAILING:3 SLIDINGWINDOW:4:15) and adapter contaminations
181 (ILLUMINACLIP option, with values 2:30:12:1:true). Reads that were shorter than 36 bases
182 after filtering were discarded (option MINLEN:36). The trimmed reads were assembled with
183 *SPAdes* (30) (version 3.7.0) with option 'careful'. The resulting contigs were used to estimate
184 the average nucleotide identity (ANI) with *dnadiff* part of *MUMmer* system (31) (version
185 3.23). The analysis included the reference genomes of *L. donovani*, *L. infantum* and *L. major*
186 that were retrieved from the Sanger database (see above), and reference genomes of *L.*
187 *braziliensis*, *L. mexicana*, and *L. panamensis* that were retrieved from ENSEMBL Protists
188 release 29 (32). The ANI values were converted to a matrix of distances, which in turn were
189 used for principal component analysis (PCA) and hierarchical clustering (R hclust function,
190 <https://www.r-project.org/>).

191

192 **Chromosome sequencing coverage.** For each read alignment file, *Samtools view* (version
193 1.3) and *BEDTools genomecov* (33) (version 2.25.0) were used to measure the sequencing
194 depth of each nucleotide. *Samtools* was run with options '-q 50 -F 1028' to discard reads
195 with low map quality score or potential duplicates, while *BEDTools genomecov* was run with
196 options '-d -split'. Nucleotide coverage was normalized by the median genomic coverage.

197 The chromosome sequencing coverage was used to evaluate aneuploidy between EP
198 and EP+3 samples. For each sample and for each chromosome the median sequencing
199 coverage was computed for contiguous windows of 2,500 bases. For those strains where
200 two EP+3 samples were available, the mean of EP+3.1 and EP+3.2 was used to calculate the

201 statistical significance of amplification compared to EP. The distribution of the median
202 window coverage in EP and EP+3 were compared with 1-way ANOVA. To have an estimate of
203 the chromosome copy number differences, the window coverage was further normalized by
204 chromosome 19 median coverage and multiplied by two. For each chromosome the median
205 values in EP and EP+3 were compared. Both the ANOVA P-values and the chromosome somey
206 comparisons are reported in **Table S4**.

207

208 **Gene sequencing coverage.** *Samtools view* (version 1.3) and *BEDTools coverage* (version
209 2.25.0) were used to measure the mean sequencing depth of every annotated gene and
210 were run respectively with options '-q 50 -F 1028' and '-d -split'. Possible intragenic gap
211 regions were excluded from the calculation of the mean. Then the mean coverage of each
212 gene was normalized by the median coverage of its chromosome. To account for GC content
213 sequencing bias, the coverage values were corrected using a LOESS regression with a 5-fold
214 cross validation to optimize the model span parameter. Genes supported by reads with a
215 mean mapping quality (MAPQ) score < 50 were filtered.

216 To enable CNV analysis of gene arrays and genes sharing high sequence identity we
217 clustered the nucleotide sequence of the annotated genes into groups with *cd-hit* (34)
218 (version 4.6). We used the length difference cutoff option '-s 0.9'. Then we realigned the
219 clusters with MAFFT (35) and used *T-Coffee seq_reformat* (36) to select a representative
220 gene per cluster (RefGene) showing the highest average sequence similarity with the other
221 cluster members. If two genes had the same average similarity then the shortest was
222 chosen. We used *bwa* to build a database containing only the sequences of RefGene, adding
223 +/- 50 base pairs of the 5' and 3' ends to ease the read alignment and the quantification of
224 small RefGenes. We realigned EP samples against this database using *bwa mem* with the

225 option '-M'. We then quantified the RefGene mean coverage (without considering the +/-50
226 base pairs extension) with *Samtools view* and *BEDTools coverage* using options '-F 1028' and
227 '-d -split', respectively. Values were normalized by the median coverage of the RefGene's
228 chromosome. Gene groups composed by members located on different chromosomes were
229 negligible and discarded.

230

231 **Genome binning.** The reference genomes were divided into contiguous windows of a fixed
232 length, and the sequencing coverage of each window was evaluated and compared across
233 different samples. A window length of 300 bases was used for the shown scatter plots
234 assessing genome-wide CNVs. Both the mean sequencing coverage normalized by the
235 median chromosome coverage and the mean read MAPQ value were computed. To account
236 for GC content sequencing bias, the coverage values were corrected using a LOESS
237 regression with a 5-fold cross validation to optimize the model span parameter. The
238 windows with MAPQ score below 50 in either EP or EP+3.1 were discarded. Poorly
239 supported windows with median or mean sequencing depth smaller than one tenth of the
240 median chromosome coverage both in EP and EP+3.1 were also discarded. The windows
241 with EP+3/EP coverage ratio outside the axes limits were placed on the edge (value of 3). In
242 the genome browser tracks the repeat elements and low complexity regions were predicted
243 with *RepeatMasker* (RepeatModeler software: Smit, AFA, Hubley, R. *RepeatModeler Open-*
244 *1.0*. 2008-2015. 2008. Available: <http://www.repeatmasker.org>) (version 4.0.6) using options
245 '-e crossmatch -gff -xsmall -s' in combination with *Repbase* (37) to identify *Leishmania-*
246 specific and ancestral repeats.

247 A window length of 2,000 bases was used for the shown circos plots assessing
248 chromosome amplification. Mean sequencing coverage and mean MAPQ score of the reads

249 aligning to that window were reported. The histogram function of *Circos* (version 0.68-1,
250 (38)) was used to visualize the coverage of the windows, using a cut off of 3. Windows with
251 mean MAPQ score below 50 or overlapping genomic gaps of over 1kb were assigned a
252 sequencing coverage of 1.

253

254 **Single nucleotide variants analysis.** To call single nucleotide variants (SNVs) we used
255 *Freebayes* (39) (version v1.0.1-2-g0cb2697) with options ‘--no-indels --no-mnps --no-complex
256 --read-mismatch-limit 3 --read-snp-limit 3 --hwe-priors-off --binomial-obs-priors-off --allele-
257 balance-priors-off --min-alternate-fraction 0.05 --min-base-quality 5 --min-mapping-quality
258 50 --min-alternate-count 2 --pooled-continuous’. The output was filtered to retain the
259 positions with just one alternate allele with a minimum frequency of 0.9, and a minimum
260 mean mapping quality of 20 for the reads supporting the reference or the alternative allele.
261 SNVs mapping inside homopolymers (i.e. simple repeats of the same nucleotide) were
262 filtered using a more stringent parameter, requiring at least 20 reads supporting the variant.
263 The homopolymers were defined as the DNA region spanning +/- 5 bases from the SNV, with
264 over 40% of identical nucleotides. We discarded SNVs with sequencing coverage above or
265 below four median absolute deviations (MADs). The predicted SNVs are reported in **Table**
266 **S5**.

267

268 **Analysis of structural variants.** *DELLY* (40) (version 0.6.7) was run with option ‘-q 50’ to
269 predict balanced structural variations, including translocations and inversion. To reduce false
270 predictions, the *DELLY* output was additionally filtered removing structural variants
271 overlapping for more than 50% of their size with either assembly gaps or repetitive
272 elements. Predictions mapping within 10kb from the telomeric ends were removed to

273 reduce false positive results caused by possible misassembled regions close to the
274 chromosome ends. Signals showing *DELLY* paired-end support of the structural variant (PE)
275 or the high-quality variant pairs score (DV) inferior to 20 were removed, as well as signals
276 showing high-quality variant pairs inferior to 20. The predicted structural variants were
277 represented with *Circos*.

278

279 **Syntenic analysis.** The syntenic analysis was performed with *SyntView* (41), a software
280 package originally designed to compare microbial genomes. The tool was adapted to browse
281 interactively the genome of four *Leishmania* reference genomes and explore their syntenic
282 relation: *L. infantum* JPCM5, *L. donovani* PBQ7IC8, *L. major* Friedlin, *L. donovani* BPK282A1.
283 This new tool hosting *Leishmania* syntenic data is publicly available at
284 <http://genopole.pasteur.fr/SynTView/flash/Leishmania/SynWebLinfantum.html>.

285

286 **Supplementary tables availability.** All supplementary tables are publicly available at:
287 https://gitlab.pasteur.fr/gbussott/Leishmania_genome_dynamics_during_environmental_adaptation_reveals_strain_specific_differences/.

289

290 **Accession number.** Reads were deposited in the Sequence Read Archive database (SRA)
291 database and are publicly available under the accession number SRP126578.

292

293

294

295 **Results**

296 **Analyzing the evolutionary relationship among *Leishmania* strains.** Ten *Leishmania* strains
297 belonging to the *L. tropica*, *L. major* or *L. donovani* complexes were obtained from different
298 sources and regions (see methods, see **Table S1**) and parasites from early and later culture
299 passages (designated EP and EP+3 respectively, **Figure S1**, **Table S2**) were subjected to
300 sequencing analysis.

301 We first used the EP sequence information to confirm species determination and to
302 characterize strain-specific genetic variations that may inform on mechanisms of adaptation.
303 PCA and clustering analyses based on the average nucleotide identity (ANI) among strains
304 confirmed the molecular determination of the various *Leishmania* species (**Figure S2 A** and
305 **B**), with *L. infantum* and *L. donovani* or *L. major* and *L. tropica* grouping together,
306 respectively. Ldo_CH33 grouped with other *L. donovani* strains, thus confirming previous
307 zymodeme analysis (17-19). Based on branch length that correlates with genetic distance,
308 the *L. infantum* isolates Linf_ZK27, Linf_LLM56, Linf_LLM45 and Linf_02A are highly related
309 as was expected by their common epidemiological classification as MON-1 (**Table S1**).

310 Comparing the repertoire of high frequency SNVs (>90%) across the *L. infantum*
311 isolates (**Figure 1A**) confirmed the very close relationship among these samples despite their
312 geographic distance, with less than 600 strain-specific SNVs observed for a given isolate. The
313 majority of SNVs shows a low frequency (data not shown), suggesting that nucleotide
314 variants may not be under strong selection in this species. In contrast, the *L. donovani* strains
315 are evolutionarily more distant as judged by the presence of over 40,000 strain-specific
316 SNVs, with high frequency SNVs likely being associated with defined haplotypes that may be
317 under selection as previously suggested (13, 42), or may be the result of geographic
318 separation and genetic drift (**Figure 1B**).

319 Finally, the SNV analysis revealed the close genetic relationship between the Tunisian
320 and Algerian *L. major* samples with 36,726 SNVs shared between the strains compared to
321 the reference genome (**Figure 1C**). The massive amount of SNVs identified in *L. tropica*
322 confirmed the large evolutionary distance to *L. major* strains observed by PCA and the
323 clustering analyses (**Figure S2**). Differences in the evolutionary relationship were further
324 supported by the absence of inversions or translocations in the *L. major* and *L. infantum*
325 strains compared to the corresponding reference genomes, and the presence of
326 translocations in the Cypriot Ldo_CH33 strain and the Sudanese *L. donovani* strain Ldo_LTB
327 (**Figure 1D**, and **Table S6**), revealing a potential role of these structural genome variation in
328 *L. donovani* adaptation.

329

330 **Strains-specific gene copy number variations.** Cross-comparing read depth among the EP
331 samples revealed important intra-species variations in copy number for single- and multi-
332 copy genes (**Table S7**, see methods). Plotting the gene coverage values for the three *L.*
333 *infantum* isolates, or the three *L. donovani* isolates, or the two *L. major* isolates together
334 with the *L. tropica* sample, resulted in strong, confined signals at the center of the ternary
335 plots that correspond to genes with equal copy number and thus a 33% distribution across
336 the three axes (**Figure 2**, left panels). Compared to the different reference genomes, we
337 observed important, strain-specific differences in gene copy number that are visualized on
338 these plots by shifts of the signals out of the centre. Overall, using a cut off of 0.5 increase or
339 decrease in normalized read depth of 1 (corresponding to the copy number per haploid
340 genome) we observed 67, 152 and 119 strain-specific amplifications for respectively *L.*
341 *infantum*, *L. donovani*, and *L. major* (**Table S8**). A selection of annotated genes is shown in

342 **Tables 1** and **2** (for the full panel see **Table S8**) and prominent examples are represented on
343 the right panels of **Figure 2**.

344 In *L. infantum* we observed (i) a 2.94-fold amplification in Linf_LLM56 of LinJ.30.2990
345 encoding for a glyceraldehyde 3-phosphate dehydrogenase, (ii) a cluster of seven genes
346 (Linj.29.0050 - Linj.29.0110) located in a ~23 kb region delimited by SIDER repetitive
347 elements that showed a two-fold amplification in Linf_ZK27, and (iii) the amplification (up to
348 32-fold) of the GP63 leishmanolysin cluster (LinJ.10.0490 - LinJ.10.0530) in Linf_02A. For *L.*
349 *donovani* we identified (i) a 48-fold amplification specific to Ldo_LTB of a cluster of ten genes
350 (LdBPK_350056400 - LdBPK_350057300), which includes a bipterin transporter, an RNase-
351 P, an RNA pseudouridylate synthase and a putative ribosomal L37e protein, (ii) an up to 26-
352 fold amplification in Ldo_BPK26 of a putative amastin surface glycoprotein
353 (LdBPK_340024100), and (iii) the deletion in Ldo_CH33 and partial depletion in Ldo_LTB of a
354 putative amastin-like surface protein (LdBPK_340015500). Finally, as expected from their
355 phylogenetic relationship, important differences were observed in gene CNVs between the
356 *L. tropica* and *L. major* strains, including (i) an amplification on chromosome 35 in both
357 Lmj_1948 and Lmj_A445 (respectively of 3.51 and 2.63-fold), spanning a hypothetical
358 protein (LmjF.35.0250) and the 5' of a putative GTP-ase activating protein (LmjF.35.0260), (ii)
359 an up to 6-fold amplification in Ltr_16 of a putative KU80 protein (LmjF.30.0340) flanked by
360 SIDER2 elements, and (iii) an Lmj_A445-specific amplification of a snoRNA cluster on
361 chromosome 26.

362 Together these results suggest that gene CNVs may drive or be the result of
363 adaptation of otherwise highly related *Leishmania* field isolates, causing phenotypic
364 differences with respect to stress resistance, nutrition, and infectivity as judged by gene
365 CNVs observed in heat shock proteins, transporters, and known virulence factors (see **Tables**

366 **1** and **2**). Thus gene CNV seems to shape the parasite genome and likely its pathogenic
367 potential in the field through positive (amplification) and purifying (deletion) selection,
368 potentially driving long-term adaptation to ecological constraints of local transmission
369 cycles.

370

371 **Dynamic karyotype changes during extended growth in culture.** We next assessed
372 structural genomic variations that may drive short-term environmental adaptation
373 comparing EP and EP+3 samples that evolved *in vitro* during culture adaptation. WGS and
374 read depth analysis revealed important karyotype differences between the two *in vitro*
375 passages of a given strain (intra-strain variation) and among different strains (inter-strain
376 variation). Aside an intra-chromosomal duplication at both EP and EP+3 observed in Ldo_LTB
377 spanning nearly half of chromosome 27 (453.410 bases) affecting 113 genes, changes in read
378 depth were homogenous across all chromosomes thus revealing frequent aneuploidy (**Figure**
379 **S3**). Linf_ZK27 and Ldo_LTB displayed the most stable karyotypes between EP and EP+3. As
380 judged by read depth values corresponding to integer or intermediate chromosome copy
381 number values, full or mosaic aneuploidy was observed for four (chromosome 6, 9, 31, 35
382 for Linf_ZK27) and six chromosomes (chromosome 13, 15, 20, 23, 31, 33 for Ldo_LTB), which
383 were established at EP and maintained at EP+3 (**Figure 3** and **Table S4**). All other isolates
384 showed higher intra-strain karyotype instability with both gain and loss of chromosomes
385 observed between EP and EP+3. Linf_02A represented the most extreme example showing
386 significant changes in read depth for twenty-one chromosomes (**Figure 3** and **Table S4**) and
387 five chromosomes with a somy score difference higher than 0.5 compared to the disomic
388 state corresponding to 2 (**Table S4**, see methods). Overall, chromosomes 20 and 23 showed
389 the highest propensity for amplification between EP and EP+3, with different ploidy levels

390 (mosaic aneuploidy, trisomy, tetrasomy) observed in respectively nineteen and fifteen
391 samples out of twenty-five, suggesting that amplification of these chromosomes may
392 provide fitness advantage during culture adaptation for most of the strains analyzed in our
393 study.

394 With the exception of the previously reported, stable aneuploidy for chromosome 31
395 (10), the dynamics of the observed karyotypic changes are substantially different among all
396 isolates. It is interesting to speculate that this heterogeneity reflects individualized solutions
397 driving fitness gains *in vitro*. While differences in culture conditions certainly account for
398 some of the observed karyotypic variability, the comparison of two closely related Spanish *L.*
399 *infantum* isolates Linf_LLM45 and Linf_LLM56 reveals a culture-independent component
400 implicated in genomic adaptation. Both isolates were adapted to culture at the same time
401 under the same conditions, yet showed important differences in karyotype dynamics, with
402 only Linf_LLM56 demonstrating changes in some levels at EP+3 (**Figure 3** and **Table S4**).
403 These strains are genotypically identical (zymodeme MON-1) (**Table S1**) and are genetically
404 closely related with an average nucleotide identity of over 99.95%, suggesting that minor
405 genetic differences may have important impact on *Leishmania* karyotypic adaptation to a
406 given environment. Aside SNVs (see **Figure 1**), the difference in karyotype dynamics may be
407 linked to gene CNVs observed between the Linf_LLM45 and Linf_LLM56, which affected
408 genes implicated for example in protein translation, protein folding, or protein turnover
409 (**Table 3**).

410 Despite this remarkable plasticity of the *Leishmania* karyotype, we observed that
411 changes in chromosome number are highly reproducible in duplicate EP+3 samples that
412 were derived for *L. major* (Lmj_1948 and Lmj_A445), *L. infantum* (Linf_ZK27), *L. donovani*
413 (Ldo_BPK26) and *L. tropica* (Ltr_16) (**Figure 3**). Thus, even though karyotypic fluctuations

414 may arise in a stochastic manner - either in the host or during culture adaptation, our data
415 demonstrate that beneficial karyotypes are under strong selection during culture
416 adaptation. Significantly, the SNV frequency profiles for EP and EP+3 were largely identical,
417 ruling out the possibility that adaptation occurs through selection of sub-populations that
418 would cause important shifts in SNV frequency distribution (data not shown). Together our
419 results document the highly dynamic nature of karyotype management in *Leishmania* during
420 environmental adaptation that is likely governed by complex interactions between external
421 cues and intrinsic genetic differences.

422

423 **Dynamic variations in gene copy number during *de novo* culture adaptation.** Plotting
424 genome-wide sequencing coverage of EP+3 against EP for all annotated genes resulted in a
425 largely diagonal distribution, suggesting that there are no major CNVs between the two
426 different passages (**Figure 4A, Figure S4, Table S9**). Overall, the majority of genes were
427 scattered around a normalized coverage of 1 (corresponding to the copy number per haploid
428 genome, see methods), suggesting that their copy number matches the one in the reference
429 strains. We nevertheless observed a significant number of genes across all isolates that
430 showed coverage either below 0.5 or above two-fold, independent of culture passage, thus
431 revealing important differences between the isolates and their corresponding reference
432 genomes. This analysis uncovered a significant increase in coverage at EP+3 for all
433 chromosomes of strain Linf_02A (**Figure 4B, Table S9**), indicating some form of CNV that
434 correlated with increased culture passage. In the following, we more closely investigated the
435 structural basis of these culture-associated CNVs in Linf_02A.

436

437 **Telomeric amplification.** We partitioned the genome into contiguous windows and plotted
438 the coverage at EP or EP+3 samples, as well as the ratio between EP+3 and EP. We observed
439 a significant increase in read depth towards the telomeres in both EP and EP+3 for
440 Lmj_1948, while coverage fluctuations in EP+3 were observed for Ltr_16, Lmj_A445, and
441 Linf_02A, generating a repetitive pattern when plotting the entire genome (**Figure 5A**). The
442 observed increase in read depth is not discrete but gradual, spanning from sub-telomeric
443 regions to the telomeres and thus cannot be assigned to misannotation of the number of
444 telomeric repeats in the reference genome (that should cause a discrete but not progressive
445 increase in read depth at the telomeres only). The gradual increase in read depth supports
446 the increased gene coverage and contributes to the shift in the chromosome coverage
447 distribution we observed for strain Linf_02A at EP+3 (**Figure 4B** and **Figure 3**). We found the
448 gradual increase in read depth to be disrupted for chromosomes 7 and 13 by regions with
449 lower read depth (**Figure 5B** and **Figure S5**). According to our model, these genomic
450 elements should not be part of sub-telomeric regions and thus either reflect a strain-specific
451 recombination event or misassembly of the *L. infantum* reference genome. Synteny analysis
452 among available reference genomes showed that the disruptive sequence elements
453 observed in Linf_02A show sub-telomeric localization in *L. major* and the novel PacBio
454 generated LdBPK genome (12), revealing misassembly of these regions in the current *L.*
455 *infantum* and the previous *L. donovani* reference genomes (**Figure 5C**). This ‘diagnostic’
456 value of our result confirms that telomeric amplification is not a technical artefact, but
457 represents a non-conventional mechanism of telomeric amplification in *Leishmania* that may
458 be similar to those described in other organisms (43).

459

460 **Discussion**

461 Drawing from newly generated genome sequences of *Leishmania* clinical isolates and
462 conducting longitudinal studies *in vitro* we demonstrate the existence of strain-specific gene
463 copy number variations that may drive long-term and short-term evolutionary trajectories in
464 *Leishmania*. We show that highly related *Leishmania* isolates that evolved in different
465 regions are distinguished by both amplification and loss of genes linked to parasite
466 infectivity, such as GP63 or amastins. The fixation of these genetic alterations may not be
467 random but could potentially be the result of positive or purifying selection processes that
468 are functional and adapt parasite fitness to a given ecology or transmission cycle.
469 Identification of such genomic alterations that are under selection by the host can directly
470 inform on genetic loci that are clinically relevant. The corresponding genes may be
471 prioritized for functional genetic analysis (notably those genes that are not annotated) as
472 they may play important roles in virulence and may qualify as biomarkers with diagnostic or
473 prognostic value.

474 Monitoring genetic fluctuations using *de novo* culture as a proxy for short-term
475 environmental adaptation revealed two forms of dynamic genomic changes. First, as judged
476 by the establishment of reproducible aneuploidy profiles in duplicate cultures of a given
477 strain, chromosomal amplification is the result of selection rather than random genetic drift.
478 This result corroborates our previous observations in the *L. donovani* experimental strain
479 LD1S, where spontaneous karyotypic fluctuations generate genotypically and phenotypically
480 diverse mosaic populations that are substrate for evolutionary adaptation and fitness gain in
481 response to environmental change (13). Whether chromosomal amplification occurs *de novo*
482 during culture adaptation or reflect an initial diversity in each clinical isolate remains to be
483 established, even though the karyotype mosaicism we previously observed *in situ* in *L.*
484 *donovani* infected hamster spleen and liver favours the latter explanation (13).

485 Second, we uncovered a novel mechanism of telomeric amplification in three
486 different *Leishmania* species (*L. major*, *L. tropica* and *L. infantum*) as revealed by a
487 progressive increasing in sequencing read depth towards the chromosome ends. Non-
488 classical mechanisms of telomere maintenance have been documented in a variety of
489 eukaryotes, including (i) rolling circle replication in *Kluyveromyces lactis*, implicating extra-
490 chromosomal circular templates (44), (ii) break-induced replication in *Saccharomyces*
491 *cerevisiae* involving recombination between tracts of telomeric repeats (45), or (iii) telomeric
492 loop formation first observed in human and mouse cells, where a telomere 3' end loops back
493 to invade the duplex part of the same telomere and anneal with complementary telomeric
494 repeat sequence (43). Our observation of a gradual increase in read depth from large sub-
495 telomeric regions towards the chromosome ends is compatible with rolling circle replication,
496 considering the propensity of *Leishmania* to extra-chromosomal amplification (9), the
497 absence of telomeric repeats in sub-telomeric regions in Linf_02A that would allow for
498 telomeric loop formation (data not shown), and the presence of only very small telomeric
499 loops of less than 1kb in the related pathogen *Trypanosoma brucei* (46). Given that bona fide
500 amastigotes cannot be maintained or adapted to culture, our *in vitro* evolutionary
501 experiments were conducted with insect-stage promastigotes that were directly derived
502 from tissue-derived amastigotes. Thus, the various forms of genomic instability we observed
503 in our system likely drive adaptation and fitness gain in the sand fly vector. While we
504 previously documented the prevalence of chromosomal amplification in tissue amastigotes
505 (13), the presence of telomeric amplification at this stage remains to be established.

506 Our comparative genomics approach further provided a powerful tool to reveal
507 species- and strain-specific variations in genomic adaptation. Telomeric amplification was
508 only seen in three of the ten isolates, and very different karyotypic solutions were observed

509 even in closely related isolates under the same culture conditions, revealing the significance
510 of environment-independent, intrinsic factors in genomic adaptation. Using the highly
511 related Spanish isolates Linf_LLM56 and Linf_LLM45 as an example, various genetic
512 determinants may be implicated. Both strains were obtained from the same area at a short
513 time frame, suggesting a very recent common ancestor as confirmed by their genetic
514 similarity. Nevertheless, they were isolated from two stray dogs and genetic differences of
515 both mammalian and insect hosts during natural infection may have shaped the parasite
516 genomes in different ways through genotype-genotype interactions, as observed for
517 example in anopheline mosquitoes infected with *Plasmodium falciparum*, the causal agent
518 of malaria (47). Given the intrinsic instability of the *Leishmania* karyotype we observed *in*
519 *situ* during visceral infection in liver- and spleen-derived amastigotes (13), these interactions
520 may establish a very different chromosomal stoichiometry among canine isolates, which
521 then translates into the different karyotypic trajectories we observed during culture
522 adaptation. Likewise, differences in the number of single-copy genes or CNVs in multi-copy
523 gene arrays generated by intra- or extra-chromosomal amplification (9) may impact on the
524 karyotypic profile, with gene amplification alleviating the need for chromosome duplication
525 as previously suggested (10). Finally, we cannot rule out that individual SNVs in coding
526 sequences or regulatory elements 5' and 3' UTRs may impact on genomic adaptation, a
527 possibility that is supported by our previous observation of tissue-specific haplotype
528 selection in the liver and spleen of *L. donovani* infected hamsters (13).

529 In conclusion, our results draw a complex picture of *Leishmania* genomic adaptation
530 in the field and in culture that needs to be considered in epidemiological studies that
531 correlate parasite phenotypic variability and disease outcome. Adaptation is highly
532 individualized and results from a dynamic selection process acting on genetically

533 heterogeneous parasite populations that thrive inside distinct and genetically equally
534 heterogeneous hosts (e.g. insects, rodents, humans). For environmental adaptation,
535 *Leishmania* can draw from a vast genetic landscape of spontaneous karyotypic fluctuations,
536 stochastic gene amplifications, and nucleotide polymorphisms. Our comparison of highly
537 related Spanish *L. infantum* isolates revealed that even small variations in sequence might
538 result in important differences in karyotypic adaptation. Thus, closely related isolates
539 evolving in the same epidemiological niche can attain similar levels of fitness in a highly
540 pleiotropic way using alternative genetic solutions (13). This form of pleiotropic adaptation is
541 characteristic for pathogenic microbes that maintain genetic heterogeneity and thus
542 evolvability despite strong selection. Our data indicates that *Leishmania* adopts a similar,
543 polyclonal adaptation strategy, which may strongly limit the identification of biomarkers
544 with broad clinical relevance across *Leishmania* species or even related *Leishmania* strains.
545 Future efforts need to take this complexity into account and approach the epidemiology of
546 *Leishmania* infection on an integrative level, considering genotype-genotype and
547 environment-genotype interactions, and dissecting the population structure of individual
548 isolates by single cell, direct tissue sequencing.

549

550 **Acknowledgements**

551 This study was supported by a seeding grant from the Institut Pasteur International
552 Department to the LeiSHield consortium, the EU FP7 (Kaladrug-R, contract 222895), the
553 Belgian Science Policy Office (TRIT, P7/41), the Department of Economy, Science and
554 Innovation in Flanders (ITM-SOFIB) and the Flemish Fund for Scientific Research (G.0.B81.12)
555 (J.C.D., F.D.).

556

557 **References**

558

559 1. Jun 2015. 5. A touch of Zen: post-translational regulation of the Leishmania stress
560 response. *Cell Microbiol*, 17.632-638.
561 [http://eutils.ncbi.nlm.nih.gov/entrez/eutils/elink.fcgi?dbfrom=pubmed&id=25801](http://eutils.ncbi.nlm.nih.gov/entrez/eutils/elink.fcgi?dbfrom=pubmed&id=25801803&retmode=ref&cmd=prlinks)
562 [803&retmode=ref&cmd=prlinks](http://eutils.ncbi.nlm.nih.gov/entrez/eutils/elink.fcgi?dbfrom=pubmed&id=25801803&retmode=ref&cmd=prlinks).

563 2. Apr 30 1984. 4643. Identification of an infective stage of Leishmania promastigotes.
564 *Science*, 223.1417-1419.
565 [http://eutils.ncbi.nlm.nih.gov/entrez/eutils/elink.fcgi?dbfrom=pubmed&id=67015](http://eutils.ncbi.nlm.nih.gov/entrez/eutils/elink.fcgi?dbfrom=pubmed&id=6701528&retmode=ref&cmd=prlinks)
566 [28&retmode=ref&cmd=prlinks](http://eutils.ncbi.nlm.nih.gov/entrez/eutils/elink.fcgi?dbfrom=pubmed&id=6701528&retmode=ref&cmd=prlinks).

567 3. 1994. The role of pH and temperature in the development of Leishmania parasites.
568 *Annu Rev Microbiol*, 48.449-470.
569 [http://eutils.ncbi.nlm.nih.gov/entrez/eutils/elink.fcgi?dbfrom=pubmed&id=78260](http://eutils.ncbi.nlm.nih.gov/entrez/eutils/elink.fcgi?dbfrom=pubmed&id=7826014&retmode=ref&cmd=prlinks)
570 [14&retmode=ref&cmd=prlinks](http://eutils.ncbi.nlm.nih.gov/entrez/eutils/elink.fcgi?dbfrom=pubmed&id=7826014&retmode=ref&cmd=prlinks).

571 4. 2013. 11. Proteomic and genomic analyses of antimony resistant Leishmania infantum
572 mutant. *PLoS ONE*, 8.e81899.
573 [http://eutils.ncbi.nlm.nih.gov/entrez/eutils/elink.fcgi?dbfrom=pubmed&id=24312](http://eutils.ncbi.nlm.nih.gov/entrez/eutils/elink.fcgi?dbfrom=pubmed&id=24312377&retmode=ref&cmd=prlinks)
574 [377&retmode=ref&cmd=prlinks](http://eutils.ncbi.nlm.nih.gov/entrez/eutils/elink.fcgi?dbfrom=pubmed&id=24312377&retmode=ref&cmd=prlinks).

575 5. Dec 2011. 12. Whole genome sequencing of multiple Leishmania donovani clinical
576 isolates provides insights into population structure and mechanisms of drug resistance.
577 *Genome Res*, 21.2143-2156.
578 [http://eutils.ncbi.nlm.nih.gov/entrez/eutils/elink.fcgi?dbfrom=pubmed&id=22038](http://eutils.ncbi.nlm.nih.gov/entrez/eutils/elink.fcgi?dbfrom=pubmed&id=22038251&retmode=ref&cmd=prlinks)
579 [251&retmode=ref&cmd=prlinks](http://eutils.ncbi.nlm.nih.gov/entrez/eutils/elink.fcgi?dbfrom=pubmed&id=22038251&retmode=ref&cmd=prlinks).

580 6. 2016. Plasticity of the Leishmania genome leading to gene copy number variations
581 and drug resistance. *F1000Res*, 5.2350.
582 [http://eutils.ncbi.nlm.nih.gov/entrez/eutils/elink.fcgi?dbfrom=pubmed&id=27703](http://eutils.ncbi.nlm.nih.gov/entrez/eutils/elink.fcgi?dbfrom=pubmed&id=27703673&retmode=ref&cmd=prlinks)
583 [673&retmode=ref&cmd=prlinks](http://eutils.ncbi.nlm.nih.gov/entrez/eutils/elink.fcgi?dbfrom=pubmed&id=27703673&retmode=ref&cmd=prlinks).

584 7. May 2009. 5. Gene expression modulation is associated with gene amplification,
585 supernumerary chromosomes and chromosome loss in antimony-resistant Leishmania
586 infantum. *Nucleic Acids Res*, 37.1387-1399.
587 [http://eutils.ncbi.nlm.nih.gov/entrez/eutils/elink.fcgi?dbfrom=pubmed&id=19129](http://eutils.ncbi.nlm.nih.gov/entrez/eutils/elink.fcgi?dbfrom=pubmed&id=19129236&retmode=ref&cmd=prlinks)
588 [236&retmode=ref&cmd=prlinks](http://eutils.ncbi.nlm.nih.gov/entrez/eutils/elink.fcgi?dbfrom=pubmed&id=19129236&retmode=ref&cmd=prlinks).

589 8. May 2013. 1. Telomeric gene deletion and intrachromosomal amplification in
590 antimony-resistant Leishmania. *Mol Microbiol*, 88.189-202.
591 [http://eutils.ncbi.nlm.nih.gov/entrez/eutils/elink.fcgi?dbfrom=pubmed&id=23421](http://eutils.ncbi.nlm.nih.gov/entrez/eutils/elink.fcgi?dbfrom=pubmed&id=23421749&retmode=ref&cmd=prlinks)
592 [749&retmode=ref&cmd=prlinks](http://eutils.ncbi.nlm.nih.gov/entrez/eutils/elink.fcgi?dbfrom=pubmed&id=23421749&retmode=ref&cmd=prlinks).

593 9. Jun 2014. 5. Genome-wide stochastic adaptive DNA amplification at direct and
594 inverted DNA repeats in the parasite Leishmania. *PLoS Biol*, 12.e1001868.
595 [http://eutils.ncbi.nlm.nih.gov/entrez/eutils/elink.fcgi?dbfrom=pubmed&id=24844](http://eutils.ncbi.nlm.nih.gov/entrez/eutils/elink.fcgi?dbfrom=pubmed&id=24844805&retmode=ref&cmd=prlinks)
596 [805&retmode=ref&cmd=prlinks](http://eutils.ncbi.nlm.nih.gov/entrez/eutils/elink.fcgi?dbfrom=pubmed&id=24844805&retmode=ref&cmd=prlinks).

597 10. Dec 2011. 12. Chromosome and gene copy number variation allow major structural
598 change between species and strains of Leishmania. *Genome Res*, 21.2129-2142.
599 [http://eutils.ncbi.nlm.nih.gov/entrez/eutils/elink.fcgi?dbfrom=pubmed&id=22038](http://eutils.ncbi.nlm.nih.gov/entrez/eutils/elink.fcgi?dbfrom=pubmed&id=22038252&retmode=ref&cmd=prlinks)
600 [252&retmode=ref&cmd=prlinks](http://eutils.ncbi.nlm.nih.gov/entrez/eutils/elink.fcgi?dbfrom=pubmed&id=22038252&retmode=ref&cmd=prlinks).

601 11. Jul 2014. 7. Genetic analysis of Leishmania donovani tropism using a naturally
602 attenuated cutaneous strain. *PLoS Pathog*, 10.e1004244.

- 603 <http://eutils.ncbi.nlm.nih.gov/entrez/eutils/elink.fcgi?dbfrom=pubmed&id=24992>
604 [200&retmode=ref&cmd=prlinks](http://eutils.ncbi.nlm.nih.gov/entrez/eutils/elink.fcgi?dbfrom=pubmed&id=24992).
- 605 12. Jun 23 2017. 3. Modulation of Aneuploidy in *Leishmania donovani* during Adaptation
606 to Different In Vitro and In Vivo Environments and Its Impact on Gene Expression.
607 MBio,
608 8.<http://eutils.ncbi.nlm.nih.gov/entrez/eutils/elink.fcgi?dbfrom=pubmed&id=285>
609 [36289&retmode=ref&cmd=prlinks](http://eutils.ncbi.nlm.nih.gov/entrez/eutils/elink.fcgi?dbfrom=pubmed&id=285).
- 610 13. Dec 2017. 12. Haplotype selection as an adaptive mechanism in the protozoan
611 pathogen *Leishmania donovani*. *Nat Ecol Evol*, 1.1961-1969.
612 <http://eutils.ncbi.nlm.nih.gov/entrez/eutils/elink.fcgi?dbfrom=pubmed&id=29109>
613 [466&retmode=ref&cmd=prlinks](http://eutils.ncbi.nlm.nih.gov/entrez/eutils/elink.fcgi?dbfrom=pubmed&id=29109).
- 614 14. Aug 2016. Gene expression in Kinetoplastids. *Curr Opin Microbiol*, 32.46-51.
615 <http://eutils.ncbi.nlm.nih.gov/entrez/eutils/elink.fcgi?dbfrom=pubmed&id=27177>
616 [350&retmode=ref&cmd=prlinks](http://eutils.ncbi.nlm.nih.gov/entrez/eutils/elink.fcgi?dbfrom=pubmed&id=27177).
- 617 15. Jul 15 2005. 5733. The genome of the kinetoplastid parasite, *Leishmania major*.
618 *Science*, 309.436-442.
619 <http://eutils.ncbi.nlm.nih.gov/entrez/eutils/elink.fcgi?dbfrom=pubmed&id=16020>
620 [728&retmode=ref&cmd=prlinks](http://eutils.ncbi.nlm.nih.gov/entrez/eutils/elink.fcgi?dbfrom=pubmed&id=16020).
- 621 16. Apr 22 2016. Evolutionary genomics of epidemic visceral leishmaniasis in the Indian
622 subcontinent. *Elife*,
623 5.<http://eutils.ncbi.nlm.nih.gov/entrez/eutils/elink.fcgi?dbfrom=pubmed&id=270>
624 [03289&retmode=ref&cmd=prlinks](http://eutils.ncbi.nlm.nih.gov/entrez/eutils/elink.fcgi?dbfrom=pubmed&id=270).
- 625 17. Jun 2009. 6-7. The paraphyletic composition of *Leishmania donovani* zymodeme
626 MON-37 revealed by multilocus microsatellite typing. *Microbes Infect*, 11.707-715.
627 <http://eutils.ncbi.nlm.nih.gov/entrez/eutils/elink.fcgi?dbfrom=pubmed&id=19376>
628 [262&retmode=ref&cmd=prlinks](http://eutils.ncbi.nlm.nih.gov/entrez/eutils/elink.fcgi?dbfrom=pubmed&id=19376).
- 629 18. Feb 2008. 1. *Leishmania donovani* leishmaniasis in Cyprus. *Lancet Infect Dis*, 8.6-7.
630 <http://eutils.ncbi.nlm.nih.gov/entrez/eutils/elink.fcgi?dbfrom=pubmed&id=18156>
631 [082&retmode=ref&cmd=prlinks](http://eutils.ncbi.nlm.nih.gov/entrez/eutils/elink.fcgi?dbfrom=pubmed&id=18156).
- 632 19. Mar 2009. 2. *Leishmania donovani* leishmaniasis in Cyprus. *Lancet Infect Dis*, 9.76-
633 77.
634 <http://eutils.ncbi.nlm.nih.gov/entrez/eutils/elink.fcgi?dbfrom=pubmed&id=19179>
635 [221&retmode=ref&cmd=prlinks](http://eutils.ncbi.nlm.nih.gov/entrez/eutils/elink.fcgi?dbfrom=pubmed&id=19179).
- 636 20. 2012. 2. Multilocus microsatellite typing (MLMT) of strains from Turkey and Cyprus
637 reveals a novel monophyletic *L. donovani* sensu lato group. *PLoS Negl Trop Dis*,
638 6.e1507.
639 <http://eutils.ncbi.nlm.nih.gov/entrez/eutils/elink.fcgi?dbfrom=pubmed&id=22348>
640 [162&retmode=ref&cmd=prlinks](http://eutils.ncbi.nlm.nih.gov/entrez/eutils/elink.fcgi?dbfrom=pubmed&id=22348).
- 641 21. Feb 2011. Database issue. The sequence read archive. *Nucleic Acids Res*, 39.D19-21.
642 <http://eutils.ncbi.nlm.nih.gov/entrez/eutils/elink.fcgi?dbfrom=pubmed&id=21062>
643 [823&retmode=ref&cmd=prlinks](http://eutils.ncbi.nlm.nih.gov/entrez/eutils/elink.fcgi?dbfrom=pubmed&id=21062).
- 644 22. Feb 2012. Database issue. GeneDB--an annotation database for pathogens. *Nucleic*
645 *Acids Res*, 40.D98-108.
646 <http://eutils.ncbi.nlm.nih.gov/entrez/eutils/elink.fcgi?dbfrom=pubmed&id=22116>
647 [062&retmode=ref&cmd=prlinks](http://eutils.ncbi.nlm.nih.gov/entrez/eutils/elink.fcgi?dbfrom=pubmed&id=22116).
- 648 23. Dec 07 2013. Aligning sequence reads, clone sequences and assembly contigs with
649 BWA-MEM. arXiv:13033997v1 [q-bioGN],
- 650 24. Jul 15 2009. 14. Fast and accurate short read alignment with Burrows-Wheeler
651 transform. *Bioinformatics*, 25.1754-1760.

- 652 [http://www.ncbi.nlm.nih.gov/entrez/query.fcgi?cmd=Retrieve&db=PubMed&](http://www.ncbi.nlm.nih.gov/entrez/query.fcgi?cmd=Retrieve&db=PubMed&list_uids=19451168)
653 [p;dopt=Citation&list_uids=19451168](http://www.ncbi.nlm.nih.gov/entrez/query.fcgi?cmd=Retrieve&db=PubMed&list_uids=19451168).
- 654 25. Aug 15 2009. 16. The Sequence Alignment/Map format and SAMtools.
655 Bioinformatics, 25.2078-2079.
656 [http://eutils.ncbi.nlm.nih.gov/entrez/eutils/efetch.fcgi?dbfrom=pubmed&id=19505](http://eutils.ncbi.nlm.nih.gov/entrez/eutils/efetch.fcgi?dbfrom=pubmed&id=19505943&retmode=ref&cmd=prlinks)
657 [943&retmode=ref&cmd=prlinks](http://eutils.ncbi.nlm.nih.gov/entrez/eutils/efetch.fcgi?dbfrom=pubmed&id=19505943&retmode=ref&cmd=prlinks).
- 658 26. Jun 2011. 5. A framework for variation discovery and genotyping using next-
659 generation DNA sequencing data. Nat Genet, 43.491-498.
660 [http://eutils.ncbi.nlm.nih.gov/entrez/eutils/efetch.fcgi?dbfrom=pubmed&id=21478](http://eutils.ncbi.nlm.nih.gov/entrez/eutils/efetch.fcgi?dbfrom=pubmed&id=21478889&retmode=ref&cmd=prlinks)
661 [889&retmode=ref&cmd=prlinks](http://eutils.ncbi.nlm.nih.gov/entrez/eutils/efetch.fcgi?dbfrom=pubmed&id=21478889&retmode=ref&cmd=prlinks).
- 662 27. Sep 2010. 9. The Genome Analysis Toolkit: a MapReduce framework for analyzing
663 next-generation DNA sequencing data. Genome Res, 20.1297-1303.
664 [http://eutils.ncbi.nlm.nih.gov/entrez/eutils/efetch.fcgi?dbfrom=pubmed&id=20644](http://eutils.ncbi.nlm.nih.gov/entrez/eutils/efetch.fcgi?dbfrom=pubmed&id=20644199&retmode=ref&cmd=prlinks)
665 [199&retmode=ref&cmd=prlinks](http://eutils.ncbi.nlm.nih.gov/entrez/eutils/efetch.fcgi?dbfrom=pubmed&id=20644199&retmode=ref&cmd=prlinks).
- 666 28. 2013. From FastQ data to high confidence variant calls: the Genome Analysis Toolkit
667 best practices pipeline. Curr Protoc Bioinformatics, 43.11.10.1-33.
668 [http://eutils.ncbi.nlm.nih.gov/entrez/eutils/efetch.fcgi?dbfrom=pubmed&id=25431](http://eutils.ncbi.nlm.nih.gov/entrez/eutils/efetch.fcgi?dbfrom=pubmed&id=25431634&retmode=ref&cmd=prlinks)
669 [634&retmode=ref&cmd=prlinks](http://eutils.ncbi.nlm.nih.gov/entrez/eutils/efetch.fcgi?dbfrom=pubmed&id=25431634&retmode=ref&cmd=prlinks).
- 670 29. Aug 01 2014. 15. Trimmomatic: a flexible trimmer for Illumina sequence data.
671 Bioinformatics, 30.2114-2120.
672 [http://eutils.ncbi.nlm.nih.gov/entrez/eutils/efetch.fcgi?dbfrom=pubmed&id=24695](http://eutils.ncbi.nlm.nih.gov/entrez/eutils/efetch.fcgi?dbfrom=pubmed&id=24695404&retmode=ref&cmd=prlinks)
673 [404&retmode=ref&cmd=prlinks](http://eutils.ncbi.nlm.nih.gov/entrez/eutils/efetch.fcgi?dbfrom=pubmed&id=24695404&retmode=ref&cmd=prlinks).
- 674 30. Jun 2012. 5. SPAdes: a new genome assembly algorithm and its applications to single-
675 cell sequencing. J Comput Biol, 19.455-477.
676 [http://eutils.ncbi.nlm.nih.gov/entrez/eutils/efetch.fcgi?dbfrom=pubmed&id=22506](http://eutils.ncbi.nlm.nih.gov/entrez/eutils/efetch.fcgi?dbfrom=pubmed&id=22506599&retmode=ref&cmd=prlinks)
677 [599&retmode=ref&cmd=prlinks](http://eutils.ncbi.nlm.nih.gov/entrez/eutils/efetch.fcgi?dbfrom=pubmed&id=22506599&retmode=ref&cmd=prlinks).
- 678 31. 2004. 2. Versatile and open software for comparing large genomes. Genome Biol,
679 5.R12.
680 [http://eutils.ncbi.nlm.nih.gov/entrez/eutils/efetch.fcgi?dbfrom=pubmed&id=14759](http://eutils.ncbi.nlm.nih.gov/entrez/eutils/efetch.fcgi?dbfrom=pubmed&id=14759262&retmode=ref&cmd=prlinks)
681 [262&retmode=ref&cmd=prlinks](http://eutils.ncbi.nlm.nih.gov/entrez/eutils/efetch.fcgi?dbfrom=pubmed&id=14759262&retmode=ref&cmd=prlinks).
- 682 32. Feb 04 2016. D1. Ensembl Genomes 2016: more genomes, more complexity. Nucleic
683 Acids Res, 44.D574-80.
684 [http://eutils.ncbi.nlm.nih.gov/entrez/eutils/efetch.fcgi?dbfrom=pubmed&id=26578](http://eutils.ncbi.nlm.nih.gov/entrez/eutils/efetch.fcgi?dbfrom=pubmed&id=26578574&retmode=ref&cmd=prlinks)
685 [574&retmode=ref&cmd=prlinks](http://eutils.ncbi.nlm.nih.gov/entrez/eutils/efetch.fcgi?dbfrom=pubmed&id=26578574&retmode=ref&cmd=prlinks).
- 686 33. Apr 15 2010. 6. BEDTools: a flexible suite of utilities for comparing genomic
687 features. Bioinformatics, 26.841-842.
688 [http://eutils.ncbi.nlm.nih.gov/entrez/eutils/efetch.fcgi?dbfrom=pubmed&id=20110](http://eutils.ncbi.nlm.nih.gov/entrez/eutils/efetch.fcgi?dbfrom=pubmed&id=20110278&retmode=ref&cmd=prlinks)
689 [278&retmode=ref&cmd=prlinks](http://eutils.ncbi.nlm.nih.gov/entrez/eutils/efetch.fcgi?dbfrom=pubmed&id=20110278&retmode=ref&cmd=prlinks).
- 690 34. Jul 01 2006. 13. Cd-hit: a fast program for clustering and comparing large sets of
691 protein or nucleotide sequences. Bioinformatics, 22.1658-1659.
692 [http://eutils.ncbi.nlm.nih.gov/entrez/eutils/efetch.fcgi?dbfrom=pubmed&id=16731](http://eutils.ncbi.nlm.nih.gov/entrez/eutils/efetch.fcgi?dbfrom=pubmed&id=16731699&retmode=ref&cmd=prlinks)
693 [699&retmode=ref&cmd=prlinks](http://eutils.ncbi.nlm.nih.gov/entrez/eutils/efetch.fcgi?dbfrom=pubmed&id=16731699&retmode=ref&cmd=prlinks).
- 694 35. 2005. 2. MAFFT version 5: improvement in accuracy of multiple sequence alignment.
695 Nucleic Acids Res, 33.511-518.
696 [http://eutils.ncbi.nlm.nih.gov/entrez/eutils/efetch.fcgi?dbfrom=pubmed&id=15661](http://eutils.ncbi.nlm.nih.gov/entrez/eutils/efetch.fcgi?dbfrom=pubmed&id=15661851&retmode=ref&cmd=prlinks)
697 [851&retmode=ref&cmd=prlinks](http://eutils.ncbi.nlm.nih.gov/entrez/eutils/efetch.fcgi?dbfrom=pubmed&id=15661851&retmode=ref&cmd=prlinks).
- 698 36. Sep 08 2000. 1. T-Coffee: A novel method for fast and accurate multiple sequence
699 alignment. J Mol Biol, 302.205-217.
700 [http://www.ncbi.nlm.nih.gov/entrez/query.fcgi?cmd=Retrieve&db=PubMed&](http://www.ncbi.nlm.nih.gov/entrez/query.fcgi?cmd=Retrieve&db=PubMed&dopt=Citation&list_uids=10964570)
701 [p;dopt=Citation&list_uids=10964570](http://www.ncbi.nlm.nih.gov/entrez/query.fcgi?cmd=Retrieve&db=PubMed&dopt=Citation&list_uids=10964570).

- 702 37. 2005. 1-4. Repbase Update, a database of eukaryotic repetitive elements. *Cytogenet*
703 *Genome Res*, 110.462-467.
704 [http://eutils.ncbi.nlm.nih.gov/entrez/eutils/elink.fcgi?dbfrom=pubmed&id=16093](http://eutils.ncbi.nlm.nih.gov/entrez/eutils/elink.fcgi?dbfrom=pubmed&id=16093699&retmode=ref&cmd=prlinks)
705 [699&retmode=ref&cmd=prlinks](http://eutils.ncbi.nlm.nih.gov/entrez/eutils/elink.fcgi?dbfrom=pubmed&id=16093699&retmode=ref&cmd=prlinks).
- 706 38. Sep 2009. 9. Circos: an information aesthetic for comparative genomics. *Genome Res*,
707 19.1639-1645.
708 [http://eutils.ncbi.nlm.nih.gov/entrez/eutils/elink.fcgi?dbfrom=pubmed&id=19541](http://eutils.ncbi.nlm.nih.gov/entrez/eutils/elink.fcgi?dbfrom=pubmed&id=19541911&retmode=ref&cmd=prlinks)
709 [911&retmode=ref&cmd=prlinks](http://eutils.ncbi.nlm.nih.gov/entrez/eutils/elink.fcgi?dbfrom=pubmed&id=19541911&retmode=ref&cmd=prlinks).
- 710 39. Jul 20 2012. Haplotype-based variant detection from short-read sequencing. arXiv
711 preprint arXiv:12073907 [q-bioGN],
- 712 40. Sep 15 2012. 18. DELLY: structural variant discovery by integrated paired-end and
713 split-read analysis. *Bioinformatics*, 28.i333-i339.
714 [http://eutils.ncbi.nlm.nih.gov/entrez/eutils/elink.fcgi?dbfrom=pubmed&id=22962](http://eutils.ncbi.nlm.nih.gov/entrez/eutils/elink.fcgi?dbfrom=pubmed&id=22962449&retmode=ref&cmd=prlinks)
715 [449&retmode=ref&cmd=prlinks](http://eutils.ncbi.nlm.nih.gov/entrez/eutils/elink.fcgi?dbfrom=pubmed&id=22962449&retmode=ref&cmd=prlinks).
- 716 41. Sep 22 2013. SynTVView - an interactive multi-view genome browser for next-
717 generation comparative microorganism genomics. *BMC Bioinformatics*, 14.277.
718 [http://eutils.ncbi.nlm.nih.gov/entrez/eutils/elink.fcgi?dbfrom=pubmed&id=24053](http://eutils.ncbi.nlm.nih.gov/entrez/eutils/elink.fcgi?dbfrom=pubmed&id=24053737&retmode=ref&cmd=prlinks)
719 [737&retmode=ref&cmd=prlinks](http://eutils.ncbi.nlm.nih.gov/entrez/eutils/elink.fcgi?dbfrom=pubmed&id=24053737&retmode=ref&cmd=prlinks).
- 720 42. Feb 2018. 1. Genome wide comparison of Ethiopian *Leishmania donovani* strains
721 reveals differences potentially related to parasite survival. *PLoS Genet*, 14.e1007133.
722 [http://eutils.ncbi.nlm.nih.gov/entrez/eutils/elink.fcgi?dbfrom=pubmed&id=29315](http://eutils.ncbi.nlm.nih.gov/entrez/eutils/elink.fcgi?dbfrom=pubmed&id=29315303&retmode=ref&cmd=prlinks)
723 [303&retmode=ref&cmd=prlinks](http://eutils.ncbi.nlm.nih.gov/entrez/eutils/elink.fcgi?dbfrom=pubmed&id=29315303&retmode=ref&cmd=prlinks).
- 724 43. May 2004. 4. T-loops and the origin of telomeres. *Nat Rev Mol Cell Biol*, 5.323-329.
725 [http://eutils.ncbi.nlm.nih.gov/entrez/eutils/elink.fcgi?dbfrom=pubmed&id=15071](http://eutils.ncbi.nlm.nih.gov/entrez/eutils/elink.fcgi?dbfrom=pubmed&id=15071557&retmode=ref&cmd=prlinks)
726 [557&retmode=ref&cmd=prlinks](http://eutils.ncbi.nlm.nih.gov/entrez/eutils/elink.fcgi?dbfrom=pubmed&id=15071557&retmode=ref&cmd=prlinks).
- 727 44. Jul 2002. 13. Recombinational telomere elongation promoted by DNA circles. *Mol*
728 *Cell Biol*, 22.4512-4521.
729 [http://eutils.ncbi.nlm.nih.gov/entrez/eutils/elink.fcgi?dbfrom=pubmed&id=12052](http://eutils.ncbi.nlm.nih.gov/entrez/eutils/elink.fcgi?dbfrom=pubmed&id=12052861&retmode=ref&cmd=prlinks)
730 [861&retmode=ref&cmd=prlinks](http://eutils.ncbi.nlm.nih.gov/entrez/eutils/elink.fcgi?dbfrom=pubmed&id=12052861&retmode=ref&cmd=prlinks).
- 731 45. May 2000. 4. Recombination in telomere-length maintenance. *Trends Biochem Sci*,
732 25.200-204.
733 [http://eutils.ncbi.nlm.nih.gov/entrez/eutils/elink.fcgi?dbfrom=pubmed&id=10754](http://eutils.ncbi.nlm.nih.gov/entrez/eutils/elink.fcgi?dbfrom=pubmed&id=10754555&retmode=ref&cmd=prlinks)
734 [555&retmode=ref&cmd=prlinks](http://eutils.ncbi.nlm.nih.gov/entrez/eutils/elink.fcgi?dbfrom=pubmed&id=10754555&retmode=ref&cmd=prlinks).
- 735 46. Mar 01 2001. 3. t-loops at trypanosome telomeres. *EMBO J*, 20.579-588.
736 [http://eutils.ncbi.nlm.nih.gov/entrez/eutils/elink.fcgi?dbfrom=pubmed&id=11157](http://eutils.ncbi.nlm.nih.gov/entrez/eutils/elink.fcgi?dbfrom=pubmed&id=11157764&retmode=ref&cmd=prlinks)
737 [764&retmode=ref&cmd=prlinks](http://eutils.ncbi.nlm.nih.gov/entrez/eutils/elink.fcgi?dbfrom=pubmed&id=11157764&retmode=ref&cmd=prlinks).
- 738 47. Feb 11 2005. Host genotype by parasite genotype interactions underlying the
739 resistance of anopheline mosquitoes to *Plasmodium falciparum*. *Malar J*, 4.3.
740 [http://eutils.ncbi.nlm.nih.gov/entrez/eutils/elink.fcgi?dbfrom=pubmed&id=15644](http://eutils.ncbi.nlm.nih.gov/entrez/eutils/elink.fcgi?dbfrom=pubmed&id=15644136&retmode=ref&cmd=prlinks)
741 [136&retmode=ref&cmd=prlinks](http://eutils.ncbi.nlm.nih.gov/entrez/eutils/elink.fcgi?dbfrom=pubmed&id=15644136&retmode=ref&cmd=prlinks).
- 742 48. Jul 08 2016. W1. deepTools2: a next generation web server for deep-sequencing data
743 analysis. *Nucleic Acids Res*, 44.W160-5.
744 [http://eutils.ncbi.nlm.nih.gov/entrez/eutils/elink.fcgi?dbfrom=pubmed&id=27079](http://eutils.ncbi.nlm.nih.gov/entrez/eutils/elink.fcgi?dbfrom=pubmed&id=27079975&retmode=ref&cmd=prlinks)
745 [975&retmode=ref&cmd=prlinks](http://eutils.ncbi.nlm.nih.gov/entrez/eutils/elink.fcgi?dbfrom=pubmed&id=27079975&retmode=ref&cmd=prlinks).

747

748 Legends

749 **Figure 1: SNVs and translocations with respect to the reference genomes.** Venn diagrams
750 showing the number of unique and shared SNVs among three *L. infantum* strains **(A)**, three
751 *L. donovani* strains **(B)** and two *L. major* strains together with a *L. tropica* strain **(C)**. **(D)**
752 *Circos* representation of genomic translocations in samples Ldo_CH33 and Ldo_LTB
753 compared to the corresponding *L. donovani* reference genome. Connecting lines represent
754 translocations events. Black and red lines demonstrate respectively Ldo_CH33 and Ldo_LTB
755 specific translocations. Blue lines show translocations common in both stains. No inversions
756 were detected using the filtering settings indicated in the methods section. Black,
757 chromosomes; red, genes mapping on the positive strand; green, genes mapping on the
758 negative strand.

759

760 **Figure 2: Inter-strain gene CNV. (A – C)** Ternary plots showing for each gene the relative
761 abundance in the three considered strains (left panels). The axes report the fraction of the
762 normalized gene coverage in the three strains with each given point adding up to 100. Black
763 dots represent unique genes, whereas red dots indicate genes representing gene families.
764 The comparison of three *L. infantum* strains **(A)**, three *L. donovani* strains **(B)** and two *L.*
765 *major* strains together with a *L. tropica* strain **(C)** are shown. The right panels show examples
766 of detected gene copy number variations (CNVs). From top to the bottom the tracks
767 represent the sequencing depth measured in the three strains, the gene annotations and the
768 predicted repetitive elements. Coverage tracks were produced with *bamCoverage* from the
769 *deepTools* suit (48) (version 2.4.2) ignoring duplicated reads. RPKM normalization was
770 applied to render the coverage comparable across samples.

771

772 **Figure 3: Chromosome ploidy analysis.** Box plots representing the normalized sequencing
773 coverage distributions for each chromosome for the strains indicated. The lower and upper
774 edges of the box show respectively the lower quartile (i.e. 25% of nucleotides with
775 normalized coverage below that value) and upper quartile (i.e. 25% of nucleotides with
776 normalized coverage above that value). The whiskers show maximum and minimum
777 coverage values excluding outliers. Outliers are not shown to ease plot readability. Box sizes
778 reflect coverage dispersion that can be affected by sample sequencing depth, chromosomal
779 ploidy, intra-chromosomal copy number alterations, assembly gaps or repetitive regions.
780 The increased box size visible in chromosome 27 of sample Ldo_LTB is caused by a large sub-
781 chromosomal amplification (see **Figure S3**). In *L. donovani*, *L. major* or *L. tropica* samples, the
782 presence of large gaps or repetitive regions inflate the box size for chromosomes 2, 8 and
783 12. Green, early passage EP; orange, EP+3.1 replicate; purple, EP+3.2 replicate.

784

785 **Figure 4: Gene copy number variation (CNV) in culture adaptation. (A)** Genome-wide
786 scatter plot showing Log₁₀ gene coverage of EP and EP+3 samples. Dots represent all genes
787 annotated in the respective reference assemblies. **(B)** Chromosome-specific scatter plots of
788 gene CNV between EP+3 versus EP. Only selected chromosomes are shown and the full
789 panel is available in **Figure S4**. The red diagonal lines indicate the bisectors. The gray dashed
790 horizontal lines mark a coverage value of 1. The axes' maximum and minimum values were
791 adjusted to the most extreme values for each individual plot to avoid logarithmic
792 compression. For both **(A)** and **(B)** the EP+3.1 replicate was used, except for Lmj_A445 for
793 which EP+3.2 replicate was utilized.

794

795 **Figure 5: Sub-telomeric amplification. (A)** Genome-wide coverage ratios (y-axes) between
796 EP and EP+3 of the indicated samples and their respective reference genomes (left and
797 middle panels) or between EP+3/EP (right panels) are shown. The EP+3 coverage refers to
798 the EP+3.1 replicate except for Lmj_A445 for which EP+3.2 replicate coverage was used. The
799 x-axis reports the position of the genomic windows along the chromosomes. Dots represent
800 genomic windows of 300 bases. In each panel the 36 *Leishmania* chromosomes are shown in
801 sequential order. To ease the visualization, all scores > 3 were assigned to a value of 3. **(B)**
802 The EP+3/EP coverage ratio for chromosomes 3, 7 and 13 of sample Linf_02A (top panel) and
803 IGV snapshots of the respective chromosome extremities (bottom panel) is shown. The
804 lower tracks (in order of appearance from the top) correspond to sequencing coverage in EP,
805 sequencing coverage in EP+3, repeat elements or predicted low complexity regions
806 predictions, and *L. infantum* gene annotations. The sequencing coverage tracks range from 0
807 to 500X. For chromosomes 7 and 13, the bottom panels highlight in orange the
808 misassembled regions. **(C)** *SyntView* snapshot of chromosomes 7 and 13. From top to
809 bottom the tracks show the orthologous genes in the *L. infantum* JPCM5, *L. donovani*
810 BPK282A1, *L. donovani* PBQ71C8 and *L. major* Friedlin. Straight lines connect the
811 orthologous genes in different genomes. The diagonal lines are indicative of misassembled
812 genomic regions.

813

814 **Supplementary Figures**

815 **Figure S1: Overview of experimental design.** Clinical isolates were obtained from infected
816 patients or dogs, placed in culture under standardized conditions and maintained for a
817 defined number of passages *in vitro*. Promastigotes from logarithmic culture at passage 2
818 (early passage EP) or passage 5 (EP+3) were subjected to sequencing analysis to monitor the

819 dynamics of genomic adaptation to the culture environment. For certain strains, two
820 independent cell cultures were derived for EP+3 to test for reproducibility of genome
821 adaptation between biological replicates (EP+3.1 and EP+3.2).

822

823 **Figure S2: Species validation.** The genomic distance between the *Leishmania* isolates used in
824 this study and the indicated *Leishmania* reference assemblies is shown by the PCA **(A)** and
825 clustering analyses **(B)**. In the PCA plot the *L. donovani* and the *L. major* clusters are
826 respectively highlighted in green and cyan.

827

828 **Figure S3: Chromosome coverage analysis.** **(A)** *Circos* plot representing the normalized
829 sequencing coverage of the strains indicated. The bar height correlates with sequencing
830 coverage. The coverage is shown on the vertical axis and ranges from 0 to 3. The ticks, scaled
831 to represent 100Kb, show the genomic position. Green, early passage EP; orange, EP+3.1
832 replicate; purple, EP+3.2 replicate. **(B)** Zoom of Lmj_1948 chromosomes 10, 11, 14, 24, 26,
833 27 and 35.

834

835 **Figure S4: Chromosome-specific gene coverage variation analysis.** For each sample and for
836 each chromosome the scatter plots show the normalized gene coverage for EP+3 (y-axis)
837 versus EP (x-axis). The red diagonal lines indicate the bisectors. To show the extent of gene
838 CNV with respect to the reference genomes, the axes limits are not fixed but dynamically
839 assigned for each chromosome to include the maximum and the minimum measured values.

840

841 **Figure S5: Chromosome-specific bin coverage variation analysis.** Dots represent adjacent
842 genomic intervals of 300 bases. For each sample, separate panels represent different

843 chromosomes. The x-axis in each panel represents the genomic coordinates while the y-axis
844 indicates the normalized sequencing coverage. Intervals with coverage superior to two are
845 highlighted in orange, and scores > 3 are assigned to 3. Intervals with coverage lower than
846 0.5 are highlighted in blue.

847

Table 1: Selection of gene CNVs in *L. infantum* field isolates (see full data in S7 Table)

<i>L. infantum</i>				
gene_id	Linf_ZK27	Linf_LLM56	Linf_02A	annotation
LinJ.08.0780	0.96	1.12	2.18	amastin-like protein
LinJ.09.0200	5.72	9.86	8.1	putative ATG8/AUT7/APG8/PAZ2
LinJ.10.0490*	18.1	20.55	32.92	GP63, leishmanolysin
LinJ.12.0661	11.63	13.46	6.1	conserved hypothetical protein
LinJ.15.1240	1.96	3.82	3.87	putative nucleoside transporter 1
LinJ.19.0820	9.58	14.39	9.09	putative ATG8/AUT7/APG8/PAZ2
LinJ.23.1330	2.45	3.44	1.46	hypothetical protein, unknown function
LinJ.26.snoRNA1	3.25	3.77	4.91	ncRNA
LinJ.26.snoRNA15	4.2	4.74	6.21	ncRNA
LinJ.26.snoRNA2	3.59	4.34	5.51	ncRNA
LinJ.26.snoRNA3	3.92	4.67	6.04	ncRNA
LinJ.26.snoRNA4	4.03	5	6.28	ncRNA
LinJ.26.snoRNA5	3.94	4.94	6.2	ncRNA
LinJ.26.snoRNA6	4.41	5.04	6.61	ncRNA
LinJ.26.snoRNA7	4.64	5.18	6.9	ncRNA
LinJ.29.0060*	2.04	1.08	0.96	putative tryptophanyl-tRNA synthetase
LinJ.29.0070*	2.17	1.02	1.01	QA-SNARE protein putative
LinJ.29.0080*	2.07	1.08	0.99	conserved hypothetical protein
LinJ.29.0090*	2.09	1.03	1.05	putative Ras-like small GTPases
LinJ.29.1610	1.89	4.45	1.81	conserved hypothetical protein
LinJ.29.2570	3.2	2.41	1.92	putative 60S ribosomal protein L13
LinJ.30.2990*	0.98	3.57	2.01	G3P dehydrogenase
LinJ.31.1470	1.98	1.96	1.17	hypothetical protein, unknown function
LinJ.31.1930	10.41	16.79	15.38	ubiquitin-fusion protein
LinJ.31.2390	1.04	1.04	0	helicase-like protein
LinJ.33.0360	20.87	13.19	12.22	heat shock protein 83-1
LinJ.34.1020	2.11	1.22	2.16	putative amastin-like surface protein
LinJ.34.1680	4.07	6.09	3.99	putative amastin-like surface protein
LinJ.36.0190	3.1	5.62	7.22	elongation factor 2

848 * , genes shown in Fig 2, right panel

849

850

851

852

853
854

Table 2: Selection of gene CNVs in *L. donovani* field isolates (see full data in S7 Table)

<i>L. donovani</i>				
gene_id	Ldo_CH33	Ldo_BPK26	Ldo_LTB	annotation
LdBPK_040006600	6.17	0.94	4.8	hypothetical protein, conserved
LdBPK_050017700	14.07	12.32	9.35	snoRNA
LdBPK_080012500	10.68	9.38	7	amastin-like protein
LdBPK_080013600	7.46	4.69	4.1	amastin-like protein
LdBPK_080015900	7.21	10.48	6.93	cathepsin L-like protease
LdBPK_090006900	8.63	4.22	9.44	putative ATG8/AUT7/APG8/PAZ2
LdBPK_100009300	4.49	15.24	5.36	folate/biopterin transporter, putative
LdBPK_120013500	10.18	7.52	18.83	surface antigen protein 2, putative
LdBPK_120014600	18.73	8.8	15.23	hypothetical protein
LdBPK_190014300	11.45	7.24	13.77	putative ATG8/AUT7/APG8/PAZ2
LdBPK_270021500	2.11	4.16	3.06	amino acid transporter, putative
LdBPK_270026500	3.24	1.13	5.69	amino acid aminotransferase, putative
LdBPK_270030100	21.94	10.67	6.68	18S,ribosomal,SSU,RNA
LdBPK_270030130	20.81	10.7	6.4	rRNA
LdBPK_270030140	21.2	10.73	6.74	28S, ribosomal,RNA,LSU-alpha
LdBPK_270030150	19.96	9.97	6.18	28S, ribosomal,RNA,LSU-beta
LdBPK_270030160	17.77	9.65	5.93	28S, ribosomal,RNA,LSU-delta,M2
LdBPK_270030170	21.2	10.74	6.19	28S, ribosomal,RNA,LSU-zeta, M6
LdBPK_270030180	17.68	10.16	5.37	28S, ribosomal,RNA,LSU-epsilon,M4
LdBPK_280010700	3.08	1.01	2.48	major surface protease gp63, putative
LdBPK_280035000	8.59	14.66	8.04	heat-shock protein hsp70, putative
LdBPK_300020900	2.34	7.56	1.88	p1/s1 nuclease
LdBPK_310009700	7.22	10.63	6.01	amastin, putative
LdBPK_310016700	4.3	8.48	5.34	sodiumstibogluconate resistance protein
LdBPK_320043700	3.28	2.02	5.44	HIBCH-like protein
LdBPK_330008700	8.56	13.64	7.76	heat shock protein 83-17
LdBPK_340015500*	0.07	1.18	0.36	amastin-like surface protein, putative
LdBPK_340015600	3.19	5.12	3.15	amastin-like surface protein, putative
LdBPK_340015800	1.78	0.92	3.36	amastin-like surfaceprotein,putative
LdBPK_340017400	2.75	1.04	0.8	amastin-like surface protein, putative
LdBPK_340023500	3.03	1.87	9.92	amastin-like surface protein, putative
LdBPK_340024100*	1.47	26.05	5.71	Amastin surface glycoprotein, putative
LdBPK_350056400*	1	1	48.78	hypothetical protein
LdBPK_350056500*	1.02	1.07	47.88	hypothetical protein, conserved
LdBPK_350056600*	1.04	0.98	44.76	Protein-only RNaseP, putative
LdBPK_350056700*	1.22	1.1	36.57	Ribosomal protein L37e, putative
LdBPK_350056800*	1.03	1.03	43.11	RNA pseudouridylate synthase, putative
LdBPK_350056900*	1.01	0.91	45.34	hypothetical protein
LdBPK_350057000*	0.92	0.96	41.41	hypothetical protein
LdBPK_350057100*	1.05	0.87	42.65	hypothetical protein, unknown function
LdBPK_350057200*	0.97	0.96	43.22	biopterin transporter, putative
LdBPK_350057300*	1.06	0.89	44	hypothetical protein

* , genes shown in Fig 2, right panel

855
856
857
858
859

Table 3: Gene CNVs in the Spanish *L. infantum* isolates Linf_LLM45 and Linf_LLM56

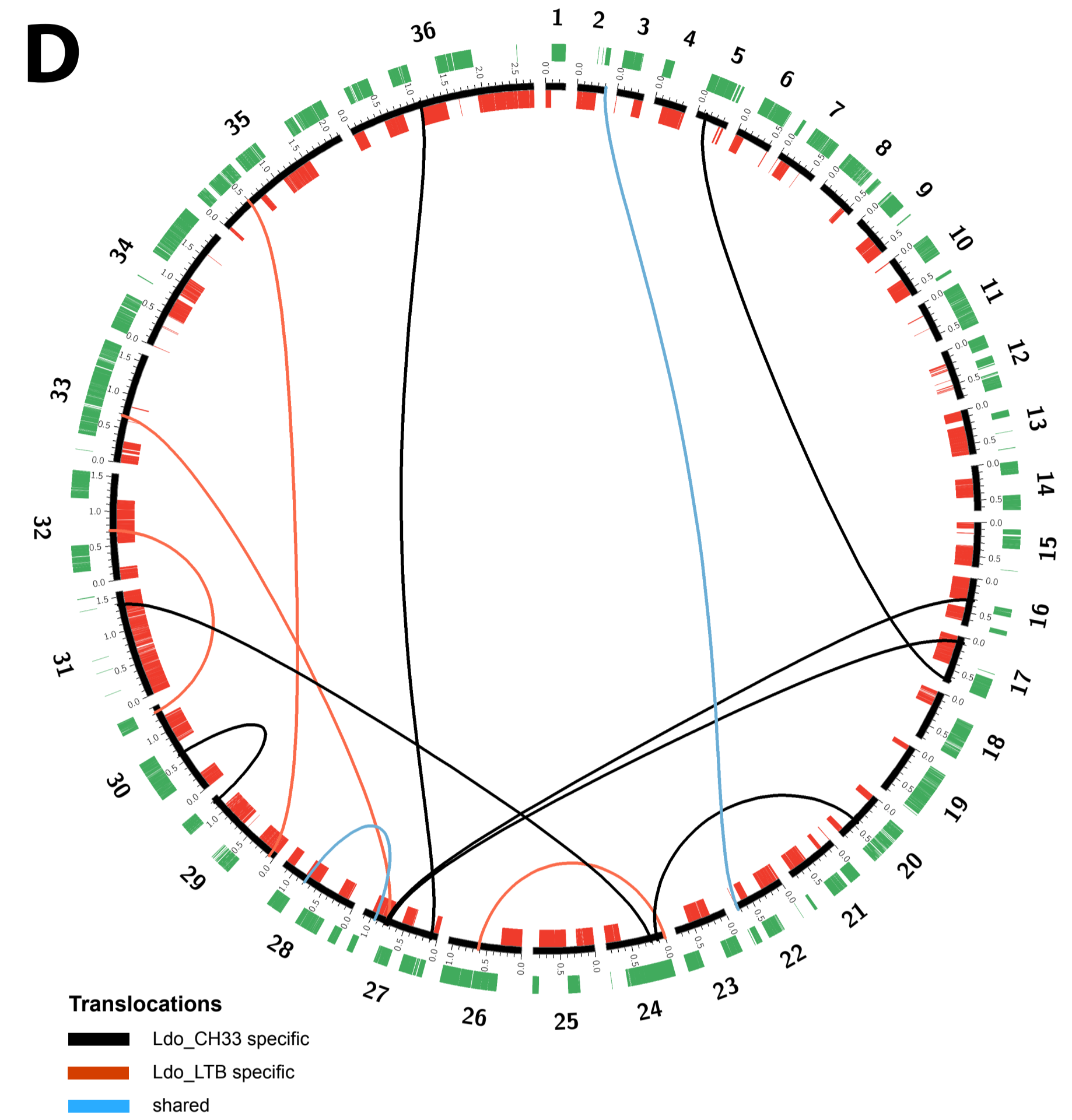
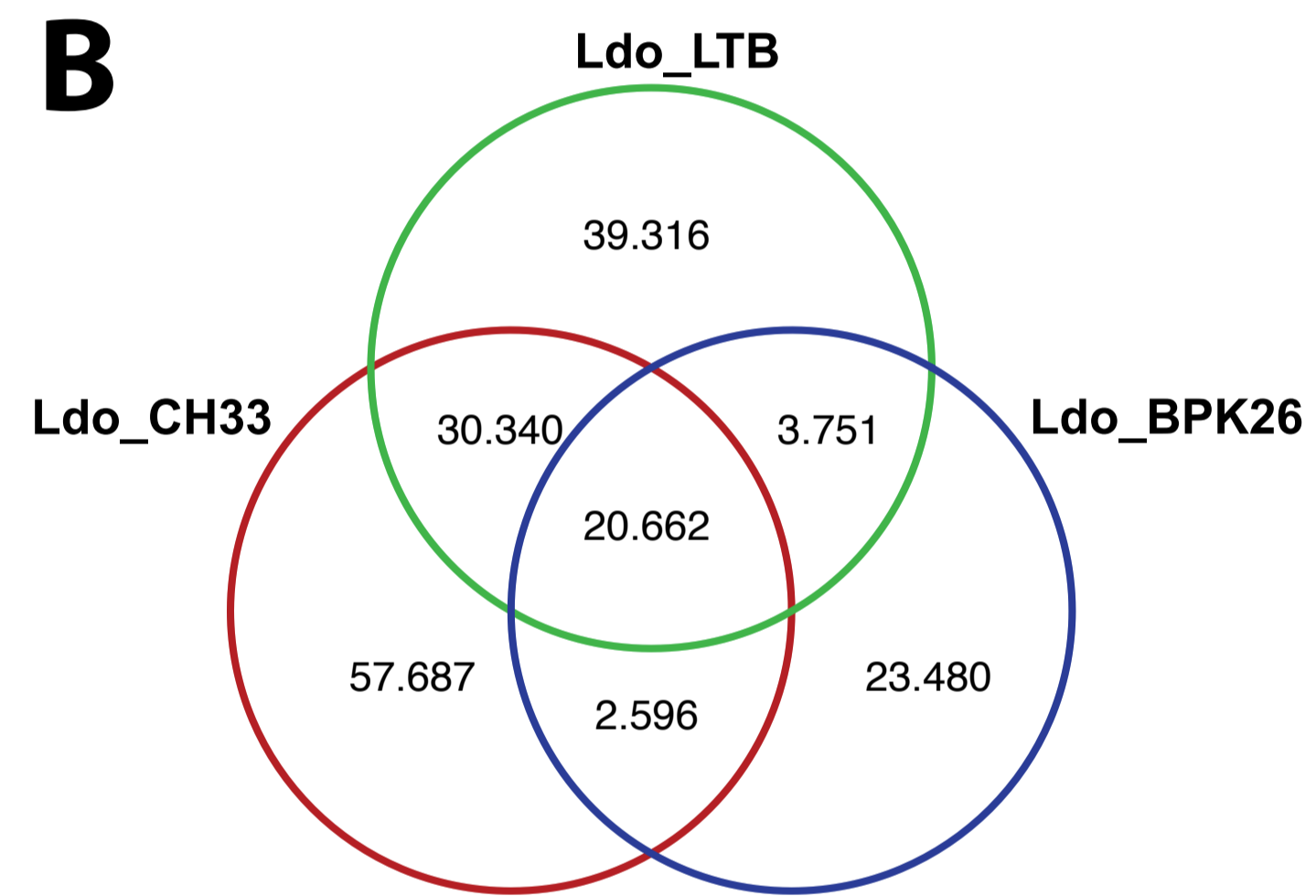
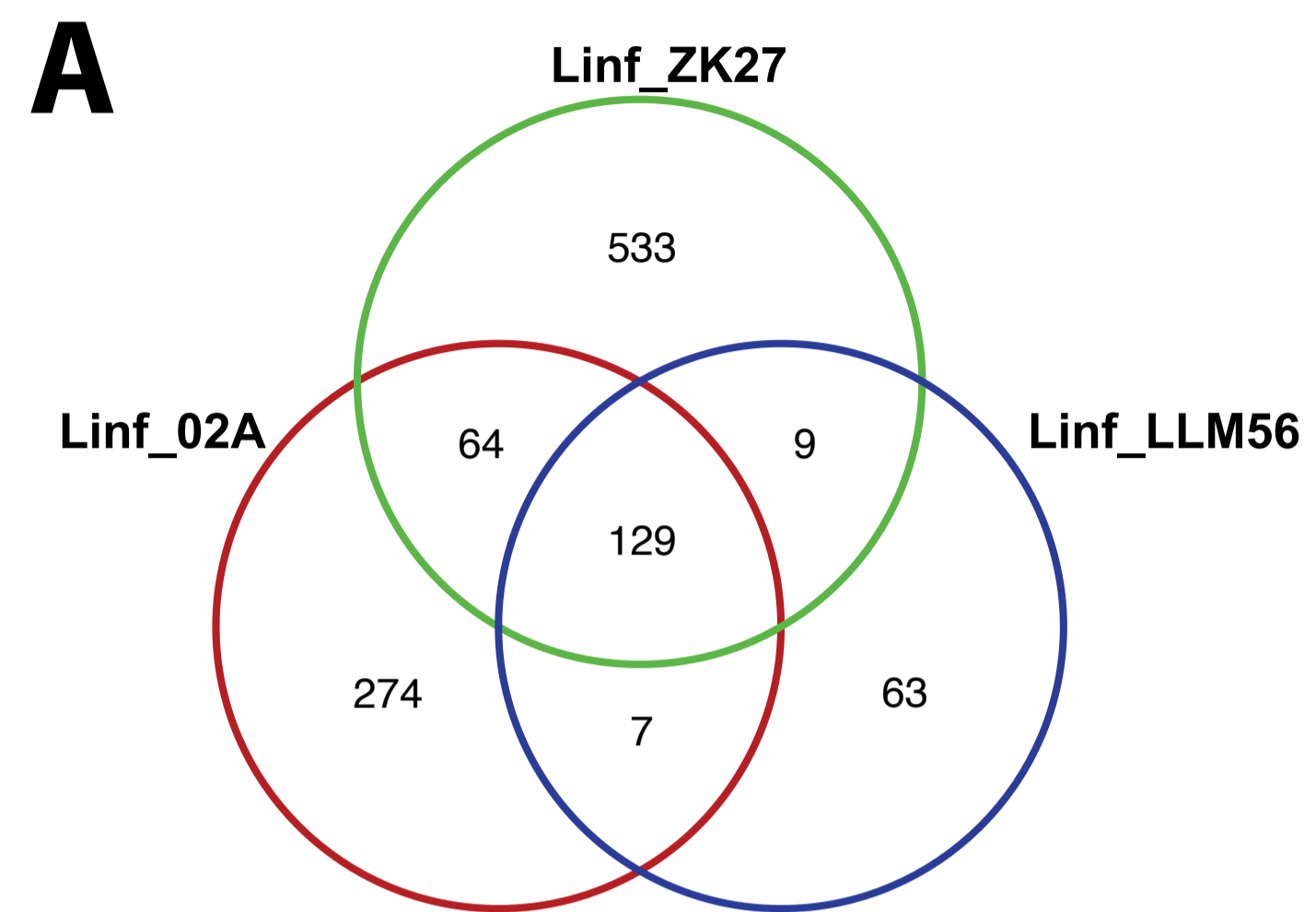
gene	45*	56*	Ratio	delta	annotation
LinJ.02.0690	1.6	2.1	0.7	0.5	hypothetical protein, unknown function
LinJ.03.0420	1.4	1.9	0.7	0.6	putative 60S acidic ribosomal protein P2
LinJ.04.0160	1.4	2.0	0.7	0.6	hypothetical protein
LinJ.04.0180	2.2	1.1	2.0	1.1	surface antigen-like protein
LinJ.05.snoRNA3	7.9	8.4	0.9	0.6	ncRNA
LinJ.05.snoRNA5	7.7	8.8	0.9	1.1	ncRNA
LinJ.09.0200	8.8	7.8	1.1	1.0	atg8 aut7 app8 paz2. Cytoskeleton
LinJ.10.0490	15.4	16.7	0.9	1.3	GP63, leishmanolysin
LinJ.11.1110	3.3	1.9	1.7	1.4	putative 60S ribosomal protein L28
LinJ.11.1120	2.1	1.0	2.1	1.1	conserved hypothetical protein
LinJ.13.0330	11.3	10.0	1.1	1.3	alpha tubulin
LinJ.14.0400	1.8	3.8	0.5	2.0	conserved hypothetical protein
LinJ.15.snoRNA4	15.3	13.8	1.1	1.5	ncRNA
LinJ.17.0090	21.1	21.8	1.0	0.8	elongation factor 1-alpha
LinJ.18.1500	4.0	3.1	1.3	0.9	putative P-type H ⁺ -ATPase
LinJ.19.0820	9.9	11.3	0.9	1.4	putative ATG8/AUT7/APG8/PAZ2
LinJ.19.1350	2.7	3.8	0.7	1.0	putative glycerol uptake protein
LinJ.22.snoRNA1	5.7	4.7	1.2	1.0	ncRNA
LinJ.26.snoRNA10	5.4	4.9	1.1	0.5	ncRNA
LinJ.26.snoRNA15	5.4	4.7	1.1	0.6	ncRNA
LinJ.26.snoRNA7	5.8	5.2	1.1	0.7	ncRNA
LinJ.29.1570	1.0	1.6	0.7	0.5	conserved hypothetical protein
LinJ.29.1580	1.0	1.5	0.7	0.5	conserved hypothetical protein
LinJ.29.1610	2.8	3.7	0.8	0.9	conserved hypothetical protein
LinJ.29.2240	1.2	1.8	0.6	0.6	conserved hypothetical protein
LinJ.30.0690	3.6	3.0	1.2	0.6	putative 40S ribosomal protein S30
LinJ.30.1660	2.0	1.4	1.4	0.6	conserved hypothetical protein
LinJ.30.3550	1.0	2.0	0.5	1.0	conserved hypothetical protein
LinJ.30.3560	1.0	2.0	0.5	1.0	S-adenosylmethioninesynthetase
LinJ.31.0460	3.0	1.0	2.9	2.0	putative amastin
LinJ.31.1660	2.9	2.1	1.4	0.8	3-ketoacyl-CoA thiolase-like protein
LinJ.31.1930	16.1	13.4	1.2	2.7	ubiquitin-fusion protein
LinJ.32.1910	2.8	1.8	1.6	1.0	putative iron superoxide dismutase
LinJ.33.0360	5.8	11.3	0.5	5.6	heat shock protein 83-1
LinJ.34.1010	5.4	3.8	1.4	1.6	putative amastin-like surface protein
LinJ.34.1020	3.1	1.2	2.6	1.9	putative amastin-like surface protein
LinJ.34.1680	4.1	6.1	0.7	2.0	putative amastin-like surface protein
LinJ.34.1730	10.9	14.4	0.8	3.5	putative amastin-like surface protein
LinJ.36.0190	6.0	5.0	1.2	1.0	elongation factor 2
LinJ.36.1680	1.8	2.5	0.7	0.6	universalminicirclesequence bd. protein
LinJ.36.3010	1.5	2.3	0.7	0.8	40S ribosomal protein S24e

861

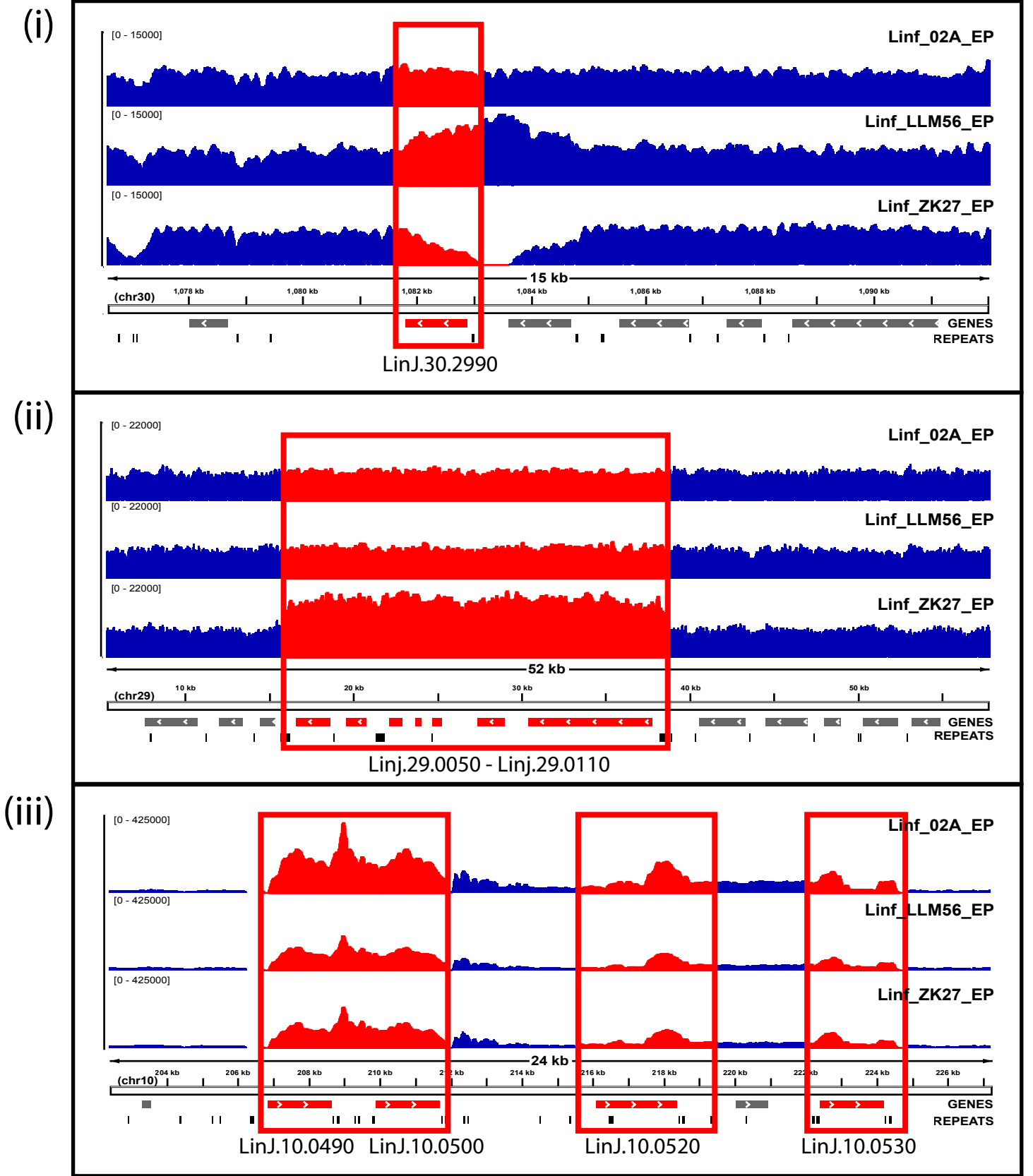
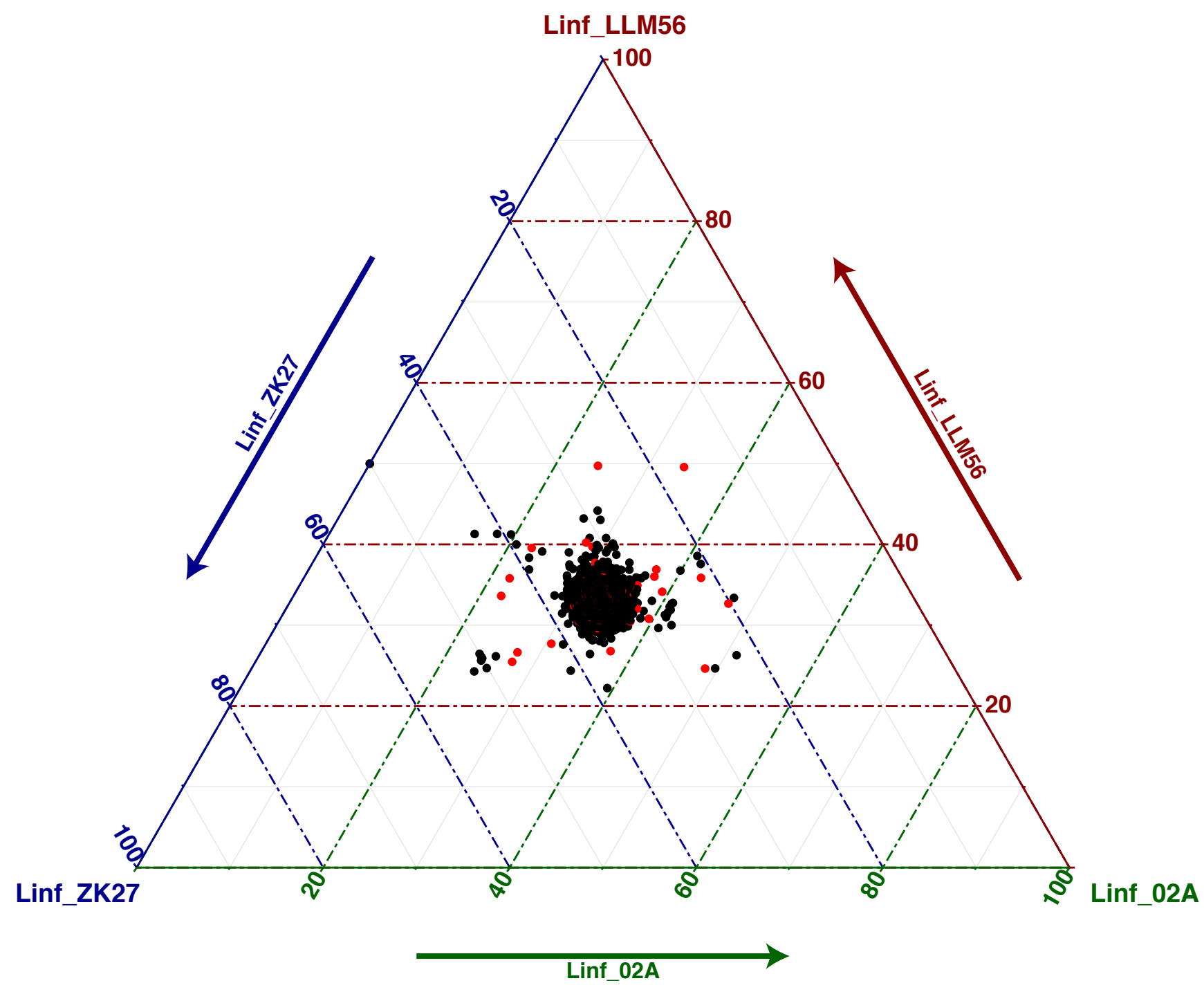
862

* normalized mean read depth of Linf_LLM45 and Linf_LLM56

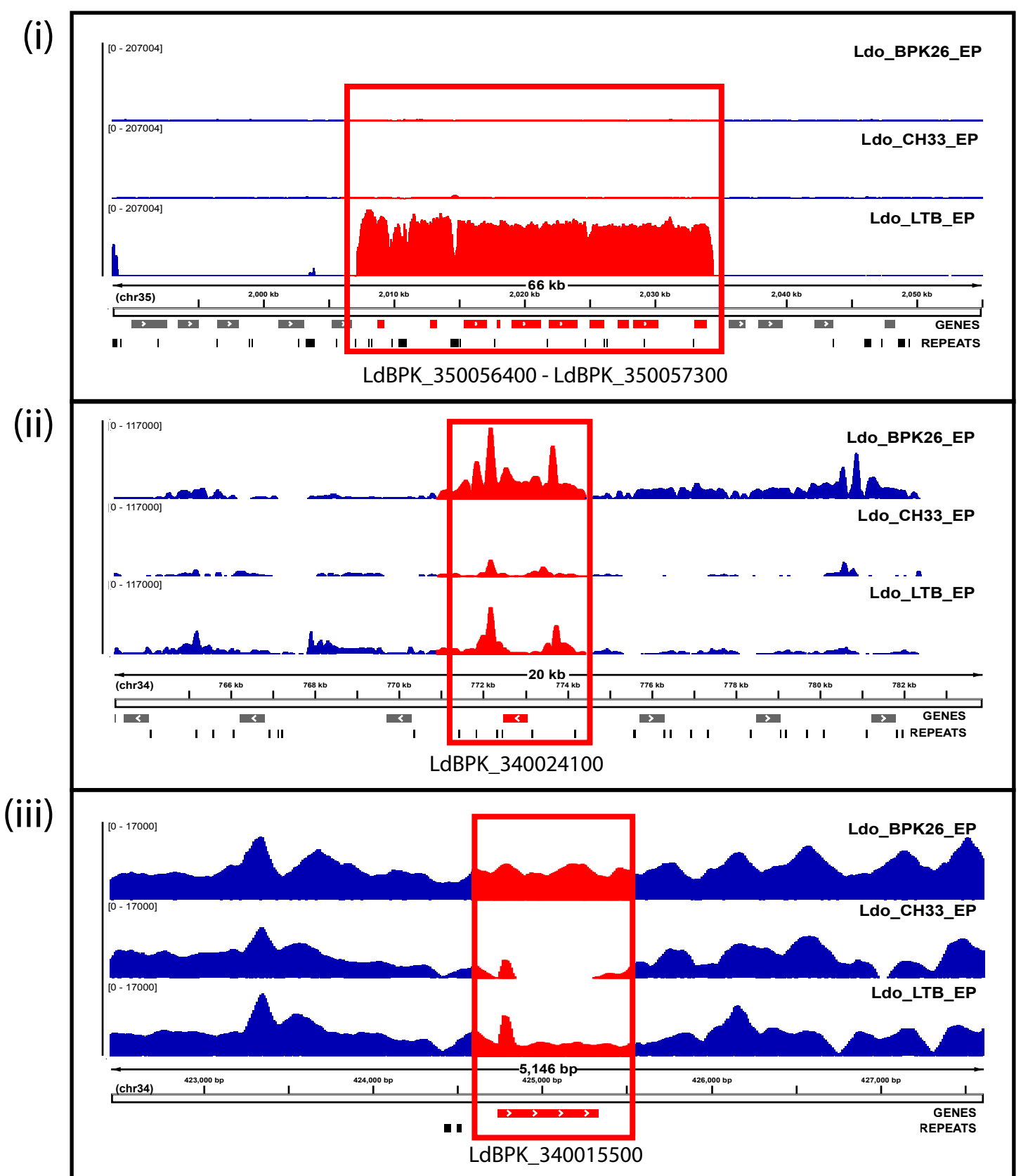
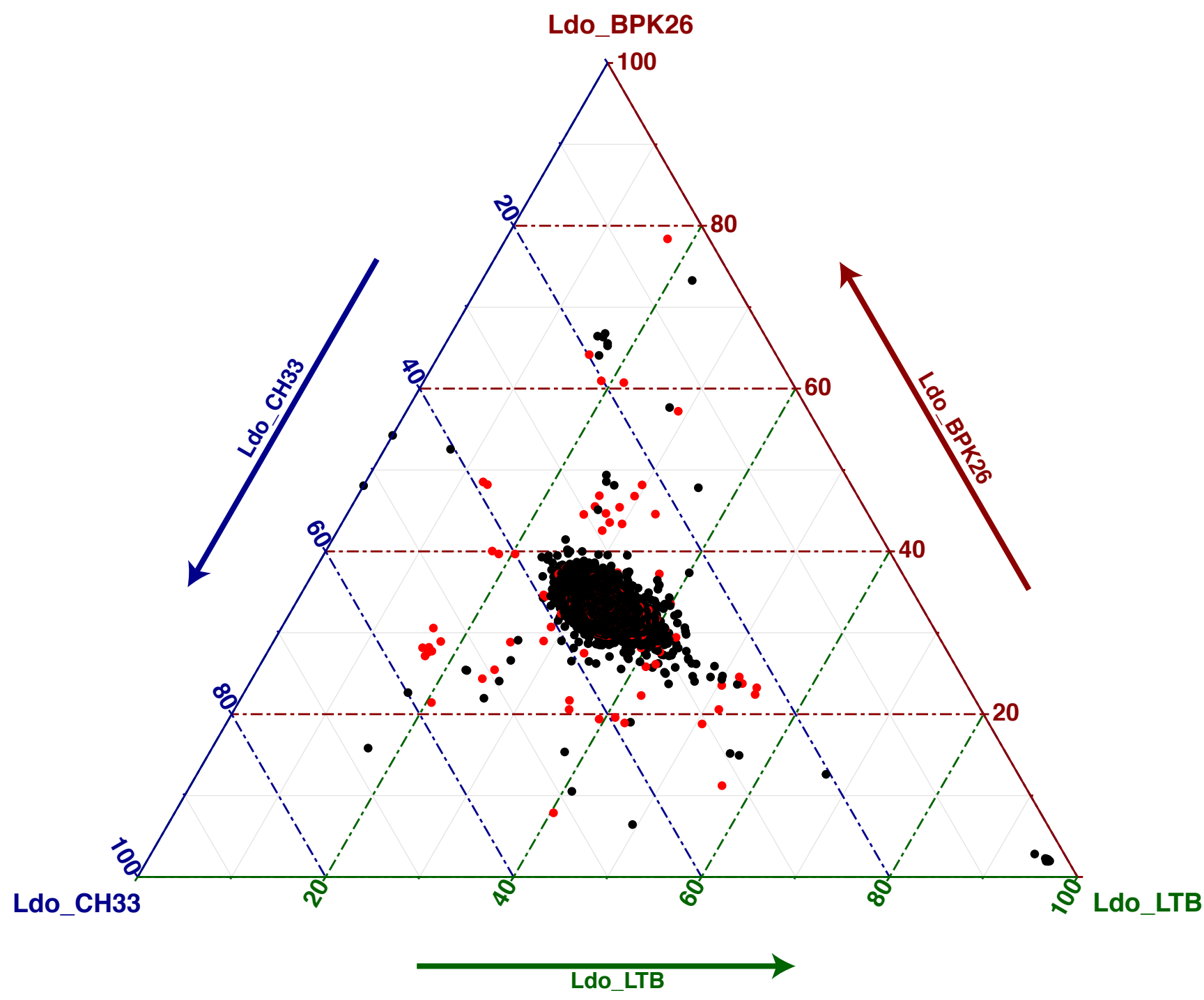
863



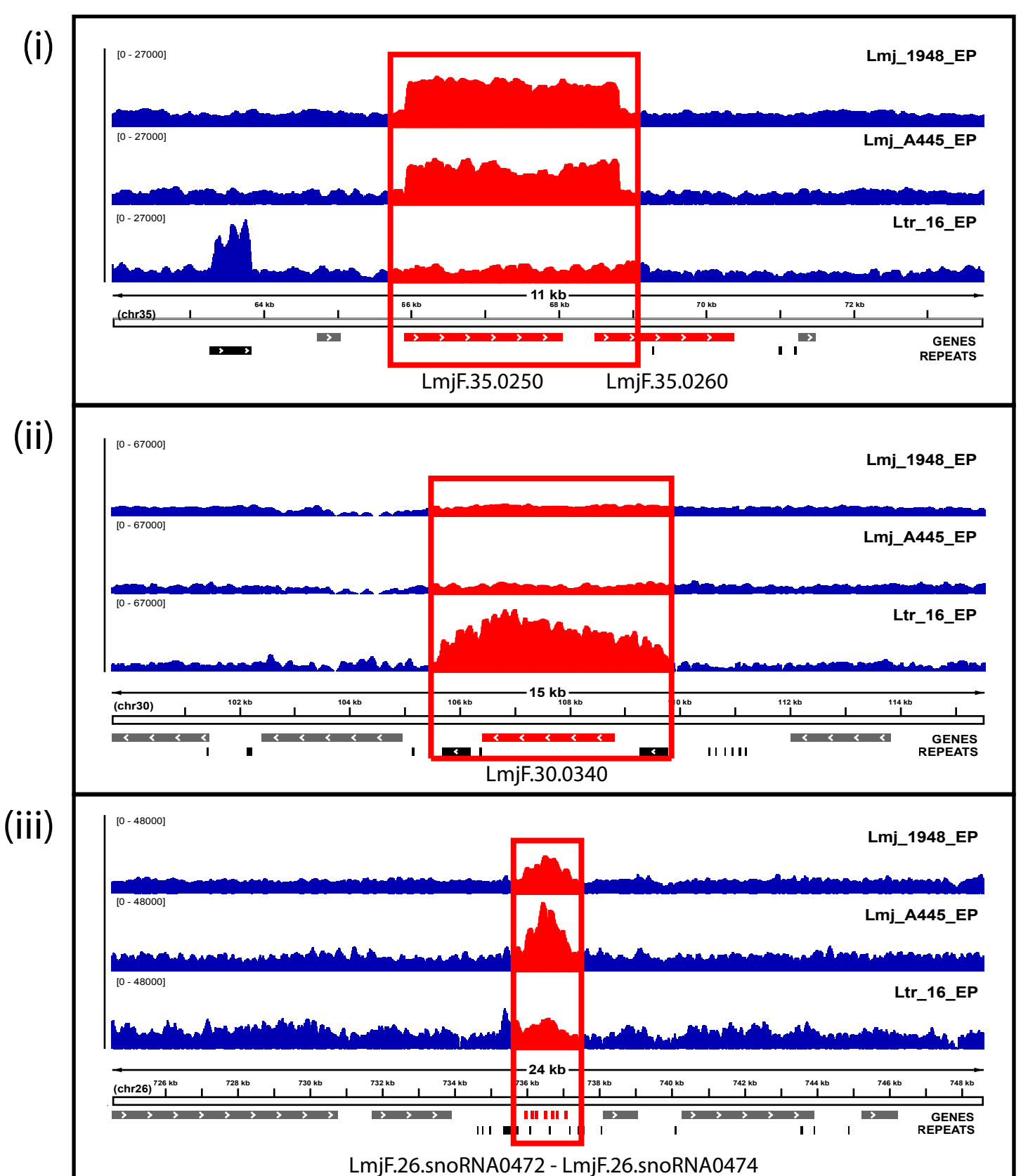
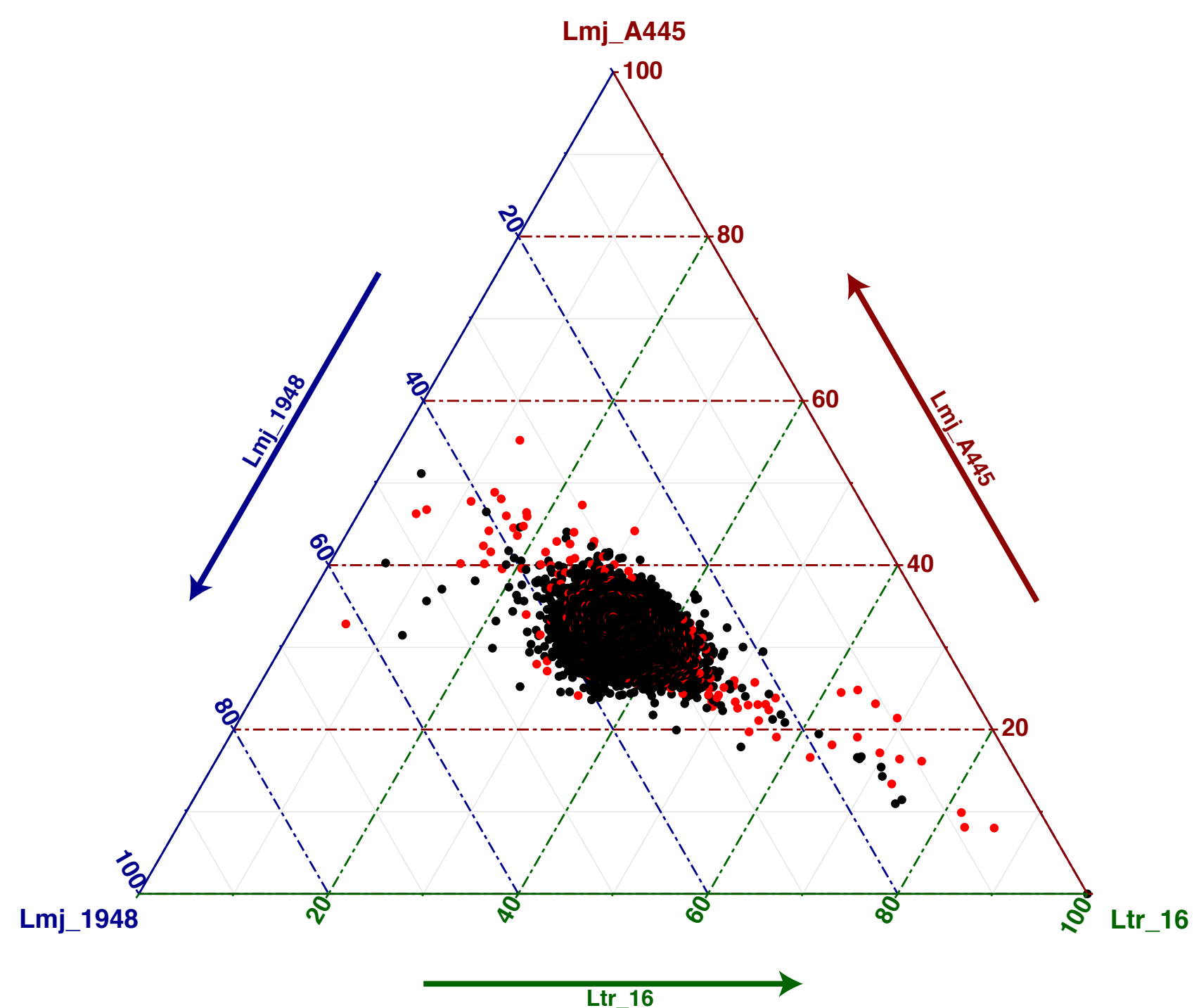
A



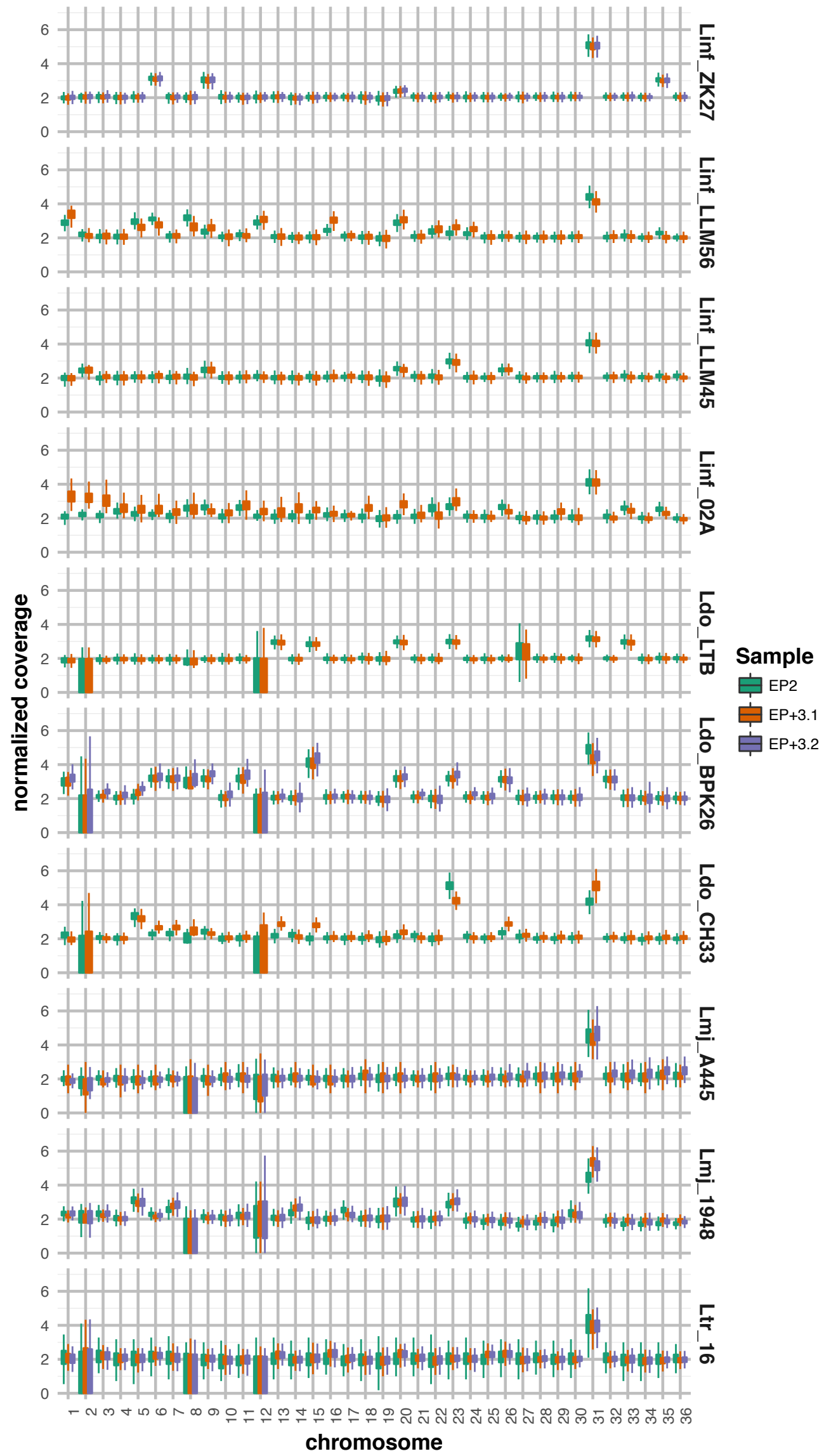
B



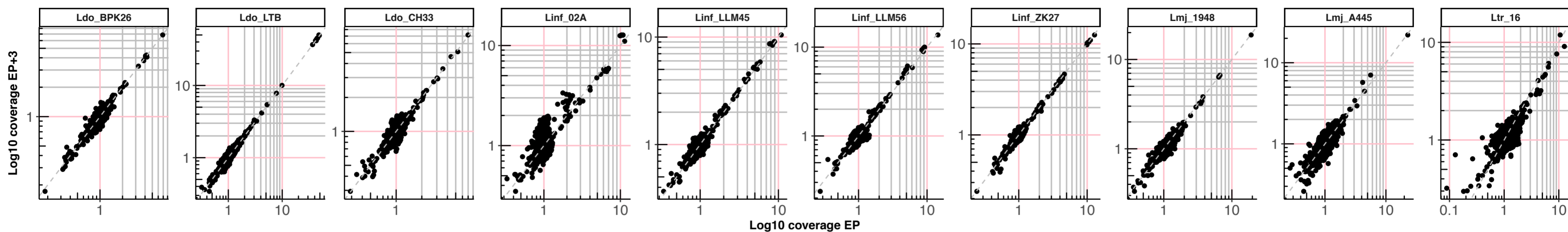
C



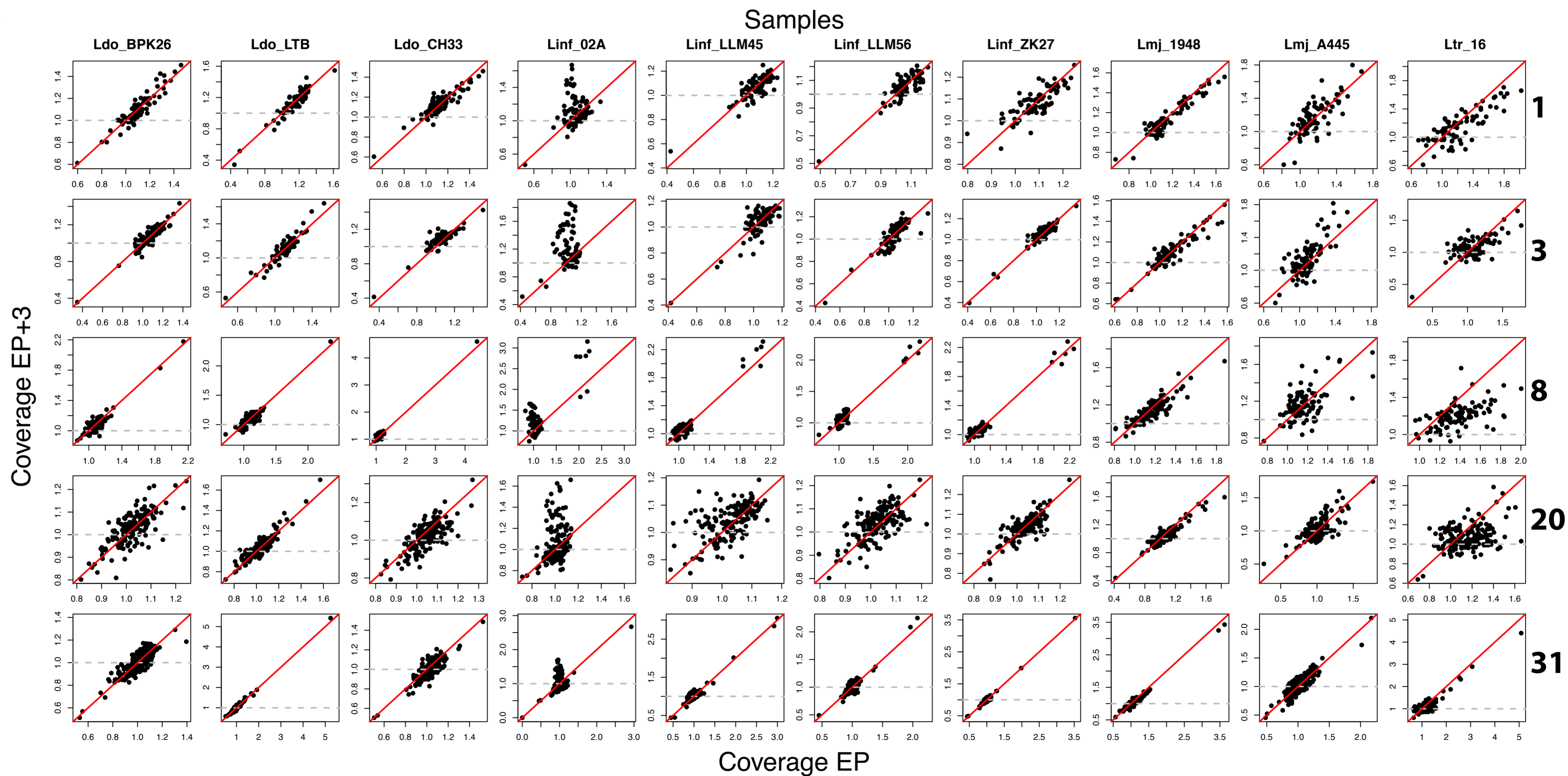
Bussotti et al_Fig3



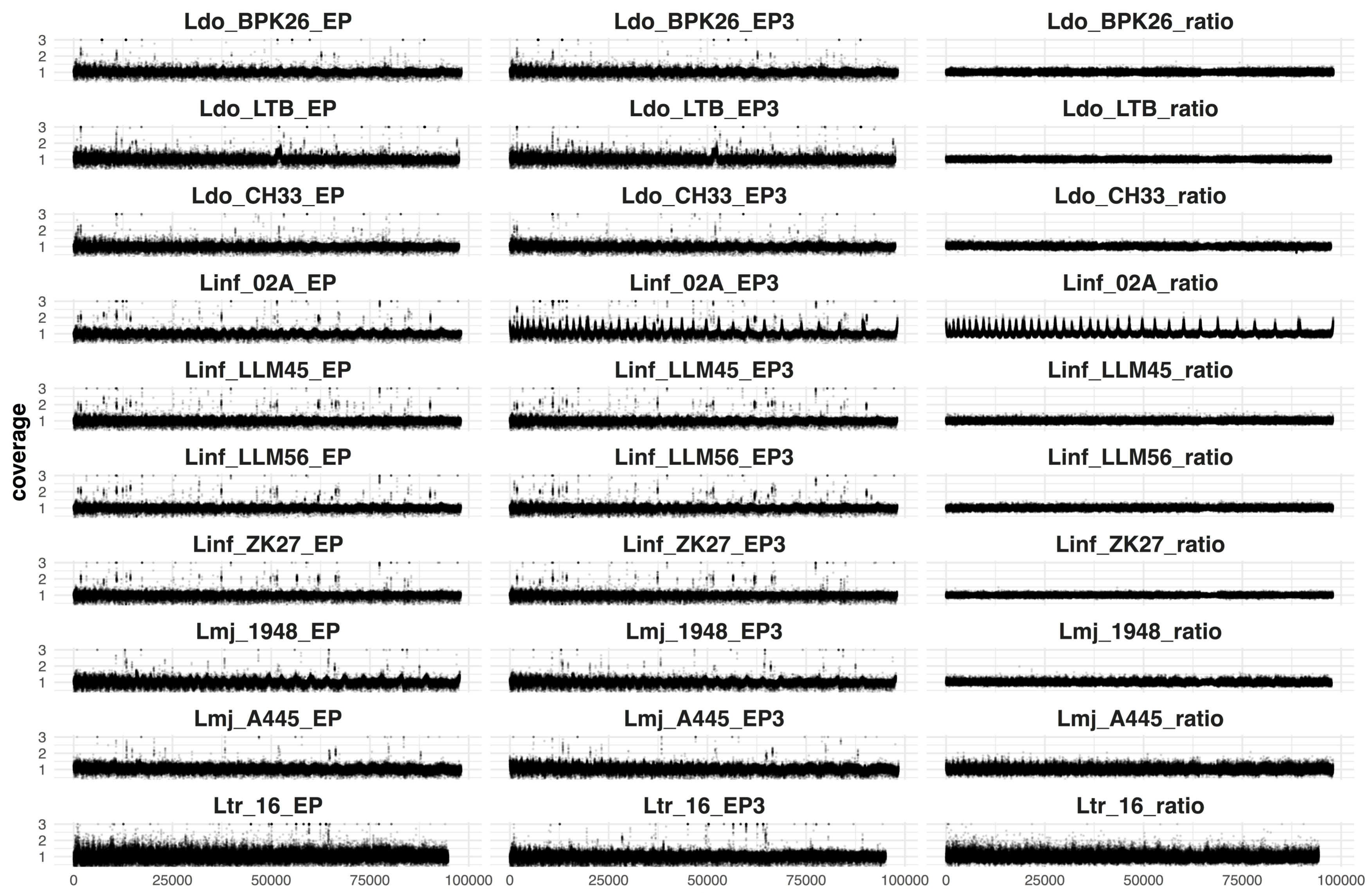
A



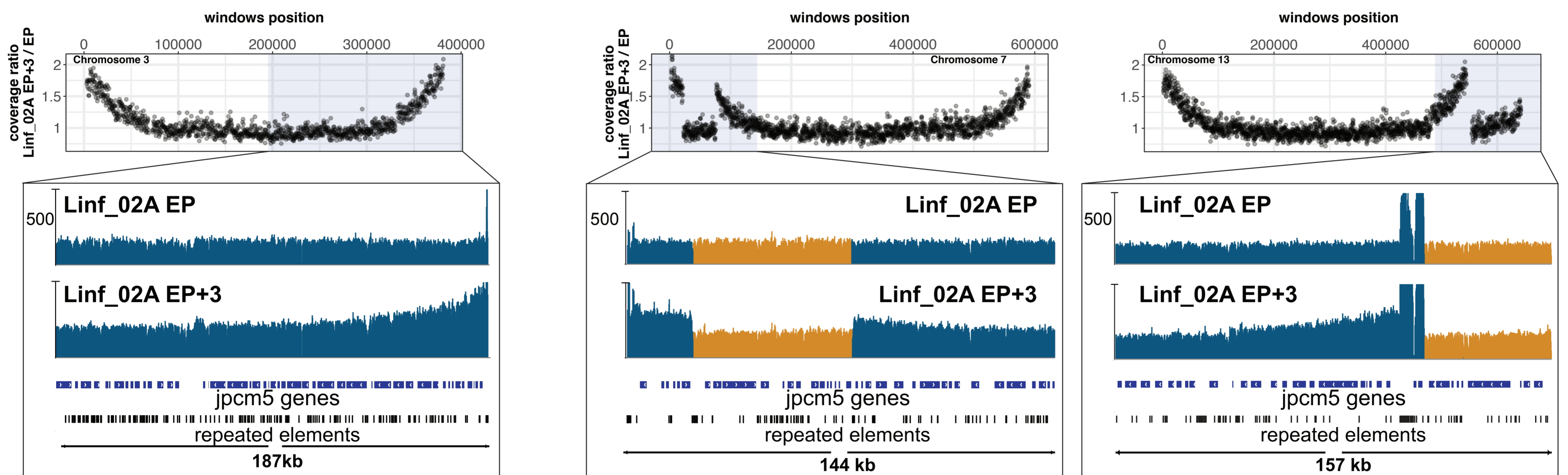
B



A



B



C

